MICROCOPY RESOLUTION TEST CHART
NATIONAL BUREAU OF STANDARDS-1963-A

②

NPS-61-84-012

NAVAL POSTGRADUATE SCHOOL
Monterey, California

DTIC
S ELECTE
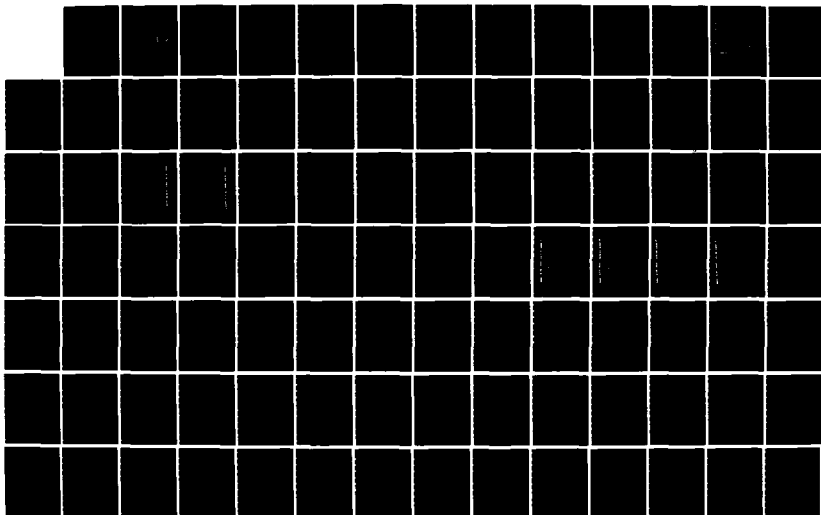DEC 20 1984
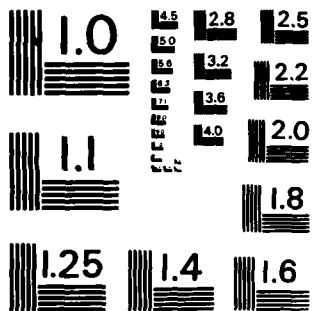D
B

MEASURED PLUME DISPERSION PARAMETERS OVER WATER

VOLUME 1

by

C. E. Skupniewicz and G. E. Schacher

SEPTEMBER 1984

Final Report for Period October 1983 - October 1984

Approved for public release; distribution unlimited

Prepared for:

Office of Naval Research

800 N. Quincy St.

Arlington, VA 22217

04

NAVAL POSTGRADUATE SCHOOL
Monterey, California

Commodore R. H. Shumaker   D. A. Schrady
Superintendent   Provost
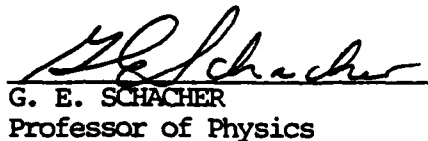
The work reported herein was supported in part by the Office of
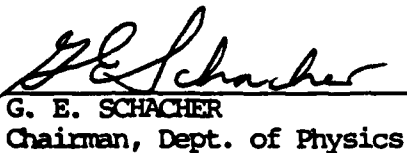Naval Research, Arlington, Virginia.

Reproduction of all or part of this report is authorized.

Tis report was prepared by:

C. E. SKUPNIEWICZ   G. E. SCHACHER
Atmospheric Scientist   Professor of Physics

Approved by:

G. E. SCHACHER
Chairman, Dept. of Physics

Released by:

J. N. DYER
Dean of Science and Engineering

REPORT DOCUMENTATION PAGE		READ INSTRUCTIONS BEFORE COMPLETING FORM
1. REPORT NUMBER NPS-61-84-012	2. GOVT ACCESSION NO. AD-A148632	3. RECIPIENT'S CATALOG NUMBER
4. TITLE (and Subtitle) Measured Plume Dispersion Parameters Over Water		5. TYPE OF REPORT & PERIOD COVERED Final Report October 83 – October 84
		6. PERFORMING ORG. REPORT NUMBER
7. AUTHOR(s) C. E. Skupniewicz and G. E. Schacher		8. CONTRACT OR GRANT NUMBER(s)
9. PERFORMING ORGANIZATION NAME AND ADDRESS Naval Postgraduate School Code 61 Monterey, CA 93943		10. PROGRAM ELEMENT, PROJECT, TASK AREA & WORK UNIT NUMBERS 61153N: rr031-03-01 N0001484WR24051
11. CONTROLLING OFFICE NAME AND ADDRESS Office of Naval Research 800 n. Quincy St. Arlington, VA 22217		12. REPORT DATE September 1984
		13. NUMBER OF PAGES 101
14. MONITORING AGENCY NAME & ADDRESS(if different from Controlling Office)		15. SECURITY CLASS. (of this report) unclassified
		15a. DECLASSIFICATION/DOWNGRADING SCHEDULE

16. DISTRIBUTION STATEMENT (of this Report)

Approved for public release; distribution unlimited

17. DISTRIBUTION STATEMENT (of the abstract entered in Block 20, if different from Report)

18. SUPPLEMENTARY NOTES

19. KEY WORDS (Continue on reverse side if necessary and identify by block number)

dispersion over water
diffusion over water
pollution
plume parameters

20. ABSTRACT (Continue on reverse side if necessary and identify by block number)

Data collected during a continuous, surface release, point source tracer experiment off the California coast is analyzed. The effects of high speed data collection from an airborne platform are removed by inverse transformation using the collecting instrument's transfer function. The tracer plume is characterized by a variety of parameters, including the conventional hourly averaged sigma-y and sigma-z values widely used in Gaussian plume dispersion formulae. Gaseous dispersion (continued)

DD FORM 1473 EDITION OF 1 NOV 68 IS OBSOLETE
1 JAN 73
S/N 0102-LF-014-6601

Item 20.   (continued)

is parameterized for the over water case by classifying the tracer results by stability in a Pasquill-Gifford equivalent scheme, and analytically describing horizontal and vertical plume growth as a function of plume travel distance.   Several other over water data sets are used in this parameterization.   Comparisons are made to the over land case.

AKNOWLEDGEMENTS

i.

MEASURED PLUME DISPERSION PARAMETERS OVER WATER

by

C. E. Skupniewicz and G. E. Schacher

(cont. p. 1)

ABSTRACT

↳ This volume analyzes the collected data.

Data collected during a continuous, surface release, point source
tracer experiment off the California coast is analyzed. The effects of
high speed data collection from an airborne platform are removed by inverse
transformation using the collecting instrument's transfer function.
in frequency space. The tracer plume is characterized by a variety of
parameters, including the conventional hourly averaged sigma-y and sigma-z
values widely used in Gaussian plume dispersion formulae. Gaseous dispersion
is parameterized for the over-water case by classifying the tracer results
by stability in a Pasquill-Gifford equivalent scheme, and analytically
describing horizontal and vertical plume growth as a function of plume
travel distance. Several other over-water data sets are used in this
parameterization. Comparisons are made to the over land case.

TABLE OF CONTENTS

INTRODUCTION

The Minerals Management Service (formerly the Bureau of Land Management) sponsored a series of four atmospheric tracer experiments at California coastal locations over a two-year span, 1980-1982. These experiments were designed to assess air pollution impact from proposed oil exploration and drilling activities along the continental shelf. Two experiments (winter and summer) at each of two sites (open coast and Santa Barbara Channel) were funded in order to investigate air quality impact under a range of meteorological conditions and sites. A brief summary of these experiments and references is supplied in Table 1.

The basic designs of all four experiments were similar. A tracer gas, 100% SF_6, was continuously released from a stationary, sea surface platform located, for the majority of the experiments, approximately 3 miles from shore. During parts of the last experiment, the platform was moved to distances up to 5 miles from shore. A variety of meteorlogical parameters were continuously monitored at various locations. Tracer gas concentrations were measured by a variety of methods at positions downwind of the release platform, with the majority made on or near the shore since the purpose was to assess potential on-shore air pollution impact. Experiments were limited to daytime periods of on-shore flow. Meteorological measurements, however, were not restricted to those time periods. This report utilizes a subset of the data base collected during the fourth experiments: offshore, aircraft,

1

Table 1

Central California Coastal Air

Quality Studies, 1981-1982

(Sponsored by Mineral Management Service)

DATE	LOCATION	FINAL REPORTS AVAILABLE	REF.*
Sep 80	Santa Barbara Channel Area	Aerovironment, Inc.	Zanetti et al. 81
Jan 81	"	"	"
Dec 81	Pismo Beach Area	Stanford Research Institute	Dabberdt et al. 83
Jun 82	"	Stanford Research Institute and Naval Postgraduate School	Dabberdt et al. 83 Other

*Other reports available.

+NPS work was sponsored by both the Minerals Management Service and the NPS Foundation Research Program.

continuous gas analyzer measurements.

The intention of this report is to characterize over-water diffusion from a continuous, near-surface, point-source release based upon these measurements. This report is built upon the meteorological results of Schacher et al. (1982) and a preliminary tracer gas and ranging results of Schacher et al. (1983). For a detailed description of the measurement techniques and data description, the reader is referenced toward these reports.

OUTLINE

A report flow chart is provided in Figure 1. This document is organized into two chapters with distinctly different designs. Chapter 1 contains technical procedures and data used in the piece-wise analysis of the data set. The second chapter presents one-hour average plume dispersion parameters, σ_y and σ_z, as a function of the well-known Pasquill-Gifford stability categories adapted for overwater use. Some additional data from other experiments supplement our data set to produce a more general parameterization.

Readers interested primarily in plume dispersion over water are advised to skip most of Chapter 1, concentrating mainly on Step 6 and Chapter 2. Those readers interested in the particular techniques used in the analysis of tracer data obtained from a high-speed platform may be more interested in Step 2. In addition to one-hour standard σ_y values, a wide variety of

3

Figure 1.

REPORT FLOW CHART

CHAPTER 1   ANALYSIS   <u>OUTPUT</u>

STEP 1. ORGANIZATION	Format data set into constant length records and include headers for each transect	IBM compatible records
STEP 2. DATA TRANSFORMATION	Apply transfer function to remove instrument response, correct for timing, rotate plume perpendicular to wind direction	spatially averaged, deconvolved individual transects
STEP 3. MISSING MINI-RANGER DATA	Apply coordinate transformations and handle passes with missing mini-ranger data	transects in fixed coordinate system
STEP 4. MULTI-MODAL GAUSSIAN FITS	Fit each pass to a multi-modal Gaussian formula and grade the analytical quality	transects represented in anal- y form
STEP 5. CALCULATIONS OF HOURLY AVERAGES	Combine meteorological and tracer data, perform range binning and hourly averages, calculate a variety of plume parameters	.ne averaged .is rsion par-ь_..ers as a function of distance from source
STEP 6. PLUME PARA-METERS AS A FUNCTION OF RANGE AND STABILITY CLASS	Perform regression analysis to derive equations defining plume parameters as a function of downwind distance and Pasquill-Gifford stability categories as applied over water	

CHAPTER 2   RESULTS

ADDITIONAL DATA SETS	Supplemental data sets obtained by other investigators are briefly described and listed	
VERTICAL DISPERSION PARAMETERS	Presentation of results	
HORIZONTAL DISPERSION PARAMETERS	Presentation of results	

analytical expressions for σ_y and σ_z as a function of stability for surface release and ranges to 10 km.

output is available from the Naval Postgraduate School Environmental Physics Group, and interested readers are advised to read Appendix A for a complete list of output data sets described throughout Chapter 1.

CHAPTER 1 - DATA ANALYSIS

Step 1 - Organization

The following data analysis was performed in a step-wise
fashion, with the complete data set stored and cataloged in the
Naval Postgraduate School's IBM 3033 mass storage system and
9-track tape at the completion of each step. Performing the
overall analysis in six separate steps allowed for manual
interrogation of the data set at each fundamental level and will
allow for easy and flexible re-analysis of the data set in the
future.

The analysis starts with SF_6 concentrations, represented as
digital voltage output from a continuous gas analyzer for single
passes through the plume. Aircraft position was recorded from
dual miniranger signals, resulting in paired position/ concentra-
tion data. Each plume transect was chosen to start where the
analyzer first sensed SF_6 along the flight path.

The original data set consists of seven files with one
experimental day per file. Each file contains a different number
of passes. Each pass starts a new (2048-byte) data block; the
number of blocks needed depends on the pass length. Records are
of variable length.

This data set was written into mass storage on the IBM 3033.
The type of mass storage file used for this analysis is called a
"partitioned data set". This data set consists of a number of
user-specified "members". Each member can be accessed interac-

6

tively or via program control. If the members are less than 5000
lines, they can be edited interactively by the user. This was
desirable; therefore, care was taken to keep each member under
this limit. Also, members must consist of 80-character records.
Therefore, the initial records became unsynchronized with the mass
storage records after the transfer.

At this point, a simple program named FORMAT converted the
variable length record format to a fixed length format. The
output was interrogated and calibration passes[+] removed.
Calibration factors derived were added to the header of each pass.
These data were written to a partitioned data set named AIR2,
residing on the Environmental Physics Group's private mass
partitioned storage volume. All data set member names, format,
and content will be presented in tabular form later in this
report.

Next, the data set AIR2 was transformed to AIR3 by the
program REDUCE. This program performed 3 vital functions.
First, it converted raw voltages (corrected for background SF_6
concentration) to parts per trillion (PPT) concentration via the
calibration factors mentioned above and experimentally-derived
calibration formulae. The calibration factors were periodically
measured during the experiment. The conversion formulae account
for instrument non-linearity at high concentrations. The
equations are:

[+] During a calibration pass, the instrument was purged with a
"span" gas of known concentration in the instrument's linear
region to obtain calibration factors.

$$V = \frac{V_B - V_0}{C} \qquad\qquad (1)$$

where V is voltage normalized to laboratory conditions;

V_0 is output voltage from the analyzer;

V_B is baseline (background) voltage;

C is the calibration factor determined during the

experiment (See Table 2).

$$SF_6 = 5340V \qquad\qquad\qquad [V < 1.345] \qquad (2a)$$

$$SF_6 = \exp(1.160V^2 - 2.455\ V + 10.122) \qquad [1.345 < V < 1.687] \quad (2b)$$

$$SF_6 = \exp(1.461V + 6.823) \qquad\qquad [1.687 < V < 2.053] \qquad (2c)$$

$$SF_6 = \exp(4.252\ V^2 - 16.780\ V + 26.369) \qquad [V > 2.053] \qquad (2d)$$

SF_6 is concentration in parts per trillion.

Table 2

Calibration Factors For Continuous SF6 Gas Analyzer

Date	Time Period (PDT)	C
6/21/82	BEGIN – 1640	.665
	1640 – END	.685
6/22/82	BEGIN – 1720	.695
	1720 – END	.685
6/24/82	BEGIN – END	.635
6/25/82	Begin – 1300	.620
	1300 – 1345	.615
	1345 – 1440	.605
	1440 – 1520	.600
	1520 – END	.615
6/27/82	BEGIN – 1720	.640
	1720 – END	.650
6/28/82	BEGIN – END	.670
6/29/82	BEGIN – 1620	.630
	1620 – END	.636

9

The second vital function performed by "REDUCE" was to determine plume transect Cartesian coordinates. This was accomplished, in most cases, with the mini-ranger data. Three scenarios existed, depending on mini-ranger performance for a given pass. When both mini-ranged distances were available, polyncminal fits were performed to eliminate data "jitter" and simple triangulation used to determine plume coordinates. When one, or both, mini-ranger signals were intermittent, regression analysis was used where possible, to fill in the "gaps". When one or both mini-ranger signals were missing, coordinate determination was postponed for later analysis. An in-depth discussion of the above process design is given in Schacher et al. (1983).

The sampling grid coordinate system is shown in Figure 2. The mini-ranger transmitters were located on the beach, and north and south buoys were located so as to aid aircraft nagivation. Their grid map locations, along with the variable ship locations are given in Table 3.

Figure 2.

NPS SF$_6$ TRACER STUDY
SAMPLING GRID
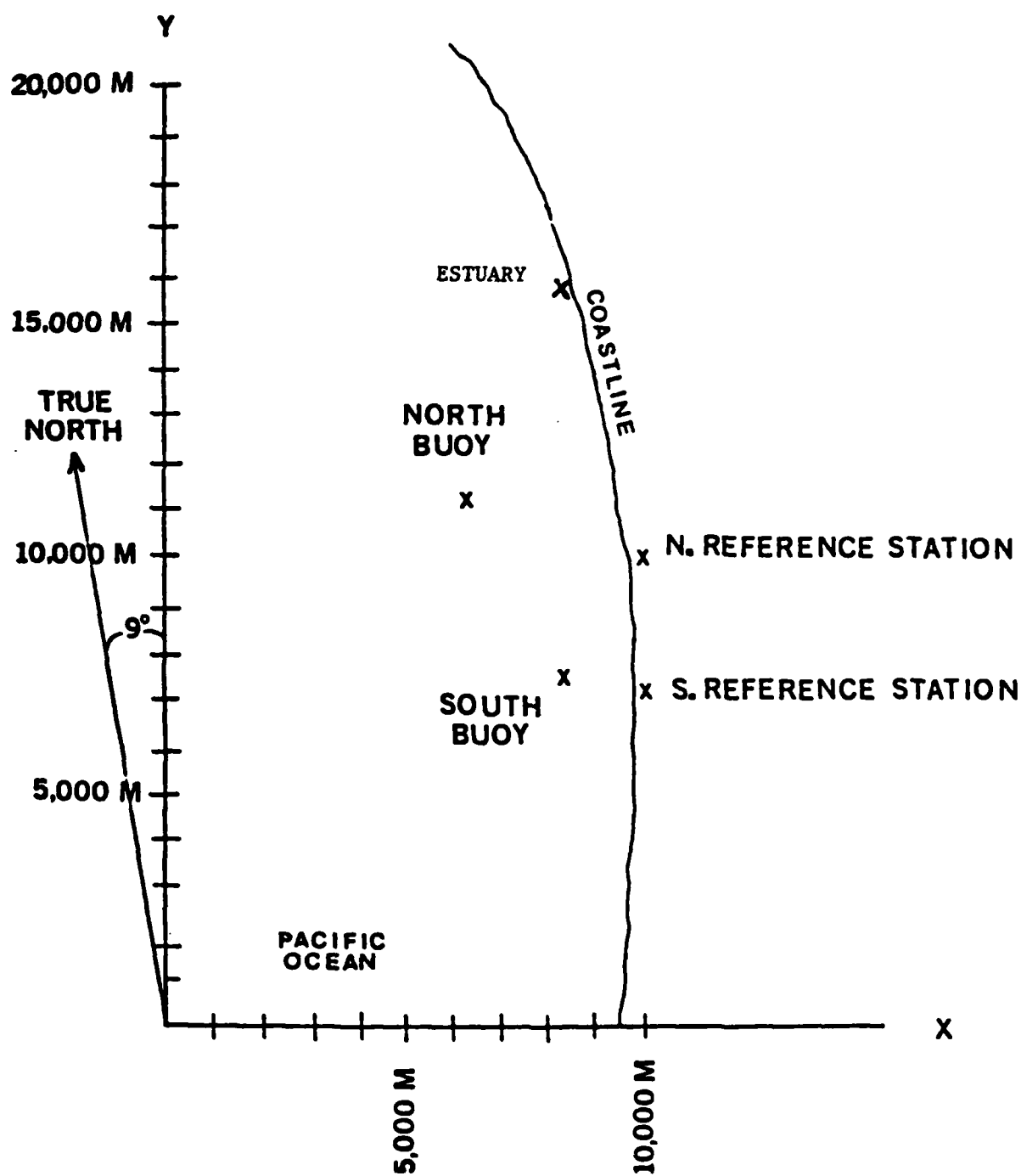
Table 3

Grid Map Locations

Reference (See Figure 2)	Grid Coordinates (meters)	
	X	Y
N. Bouy	5926	11140
S. Bouy	8114	7550
Ship 6/21/82	4055	10200
" 6/22/82	4945	6369
" 6/24/82	4103	8628
" 6/25/82	4111	8601
" 6/27/82	399	11090
" 6/28/82	581	12493
" 6/29/82	1120	10459
Estuary	8896	15430
N. Ref. Station	10000	10000
S. Ref. Station	10000	7050

Figure 3a.

MASS STORAGE DATA SET "AIR2";

ABBREVIATED SAMPLE OF ANALYSIS STEP 1 OUTPUT

INDIVIDUAL LINE KEY: column one is the code

P: date, time, pass number, data quality index, altitude
B: total elapsed time (sec), total number of points,
mini-ranger 0 number of points, mini-ranger 1 number
of points, number of bad points, calibration factor
D: mini-ranger code, distance from mini-ranger (m),
analyzer output (volts)

13

MASS STORAGE DATA SET "AIR3";

ABBREVIATED SAMPLE OF ANALYSIS STEP 1 (continued)

INDIVIDUAL LINE KEY:

    lines 1-7: header information (self explanatory)
        8-11: mini-ranger statistics
          12: R/V ACANIA position in grid (see Figure 2)
        14-: data -time in seconds
                        -width is distance from first non-zero
                         concentration in meters
                        -concentration in PPT

Step 2 - Data Transformation

This step accounts for instrument effects on the data. If the data are perceived as a time series, and we treat the instrument as a first-order linear system*, then,

$$\frac{d\tilde{X}}{dt} = \tilde{A}\tilde{X} + \tilde{B}\tilde{U} \qquad (3)$$

where $\tilde{X}$ is a one-dimensional matrix of state variables;

$\tilde{U}$ is a matrix inputs;

$\tilde{A}, \tilde{B}$ are square matrices of coefficients; and

t is the independent variable.

In general, the system output can be represented as a linear combination of the state variables and the inputs. In this specific case, the input is the true SF_6 concentration, and the output of interest is a state variable, the measured SF_6 concentration. Also, this case is concerned with only one state variable; therefore, matrix expressions will be dropped. A solution can be expressed as the convolution of the input waveform and a function called the unit impulse response of the system.

$$x(t) = {}_{-\infty}\int^{+\infty} h(t - \tau)u(\tau)d\tau \qquad (4)$$

where $x(t)$, $u(t)$ are singular state and input variables, respectively;

$h(t)$ is the unit impulse response.

---

*In a second-order system, a second state variable would simply be the derivative of the first variable.

15

Convolutions are rather difficult to perform on digital machines; therefore, we use the convolution theorem, which states that convolution in the time domain is analagous to multiplication in the frequency domain.

$$x(t) = F^{-1}[X(f)] = F^{-1}[H(f)U(f)] \qquad (5)$$

where $X(f)$ is the Fourier transform of $x(t)$

   $U(f)$ is the Fourier transform of $u(t)$

   $H(f)$ is the Fourier transform of $h(t)$, or the "transfer function"

   F^{-1} refers to the inverse Fourier transform.

Finally, since the system input is the desired quantity, Equation (5) is inverted, yielding:

$$u(t) = F^{-1}[X(f)/H(f)] \qquad (6)$$

A graphical example can serve as a "proof" of this concept, often referred to as the transfer function approach (see Figure 4). Let the unit impulse response be the unit impulse. The impulse transforms to a constant function of magnitude 1, while $x(t)$ transforms to $X(f)$. Their product is identically $X(f)$, and the inverse Fourier transform yields $x(t)$. It is obvious that any input function , $u(t)$, will produce an output, $x(t)$, identical to itself, as it should, if the system is transparent. This example should not be considered complete proof of the transfer function approach, but merely demonstrates an extreme situation.

16

Figure 4. GRAPHICAL EXAMPLE OF TRANSFER FUNCTION APPROACH AND "PROOF"
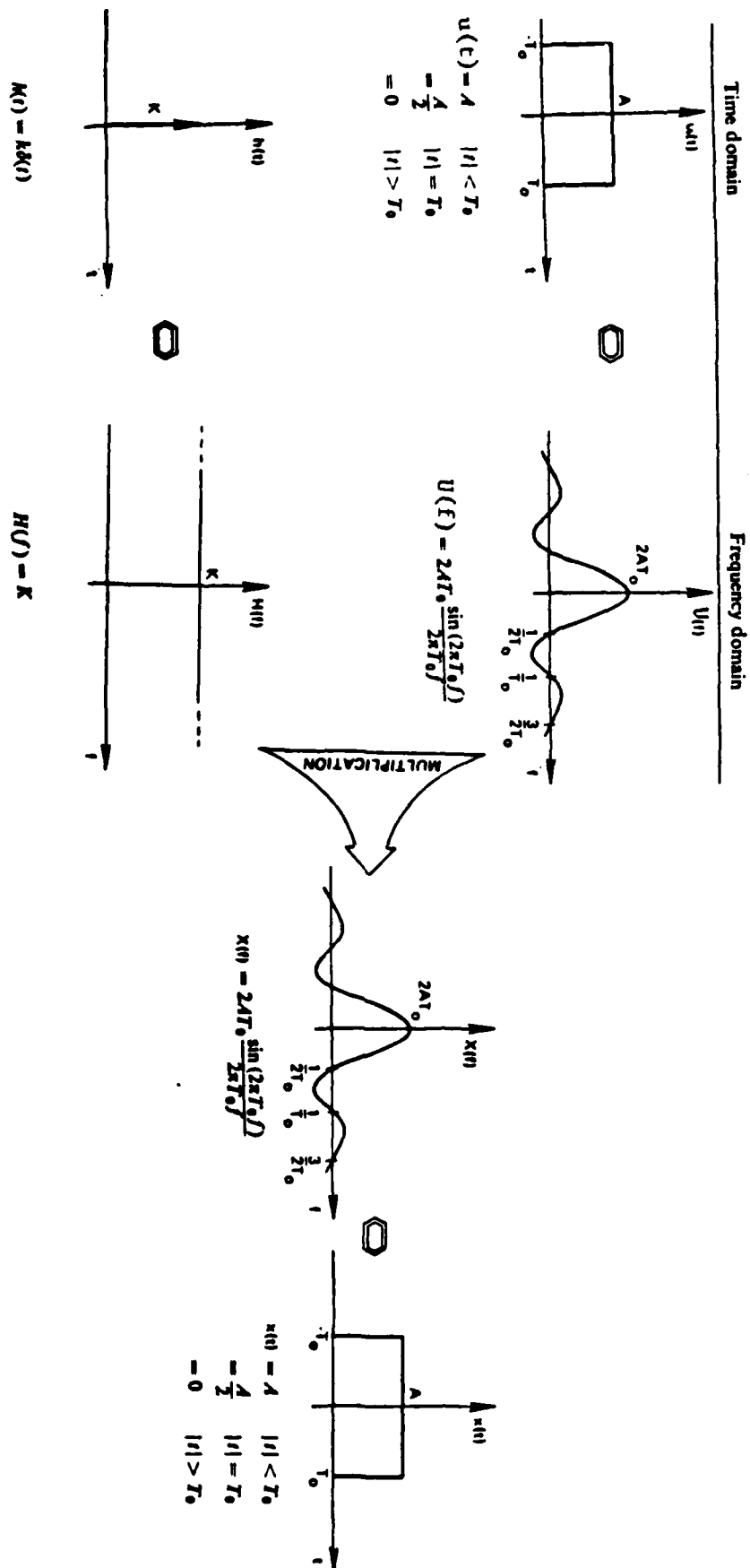
The program developed to apply the transfer function was called XFORM. The Cooley-Tukey fast Fourier transform routine was used as the core of this program. No tapers were applied to the time domain truncation function in order to reduce leakage because the frequency distribution of the waveform was unknown. All high frequency information was desirable, and a taper could have destroyed that information. Also, Hanning or cosine windows often smooth the waveform. This would art/ficially widen the plume; an undesirable effect. To keep computations to a minimum, the number of points in the discrete Fourier transform should be small. Crow and Tewscher (1983) determined the proper number to be 18, based on the instrument high frequency cut-off and the approximate airspeed. The program XFORM therefore averaged each pass into an 18 point series before applying the transform. Each point, therefore, represented upwards of 100 samples. If the measurement variability between samples is considered independent, this would decrease the statistical significance of measurement errors tenfold. Considering the nature of the noise (instrument noise, intake airflow dynamics, etc.) and the errors produced, the data density achieved in this experiment appears to be more than necessary to achieve sufficiently small error. Ten to twenty samples per data point would have produced accuracy to within 50 ppt, an acceptable level. The 18 point series was designed so that the records start and end at zero concentration, with all other points non-zero, to avoid introducing false high-frequency components due to discontinuity or background noise. The

18

untransformed data set was stored on mass storage for comparison
to the transformed data

The program XFORM next entered the transfer function subroutine.
The first task in the subroutine was to determine the transfer
function. This was accomplished by first transforming the
experimental time series; a simulated "unit impulse" as the input
waveform, and the resultant measured SF_6 concentration as the
output. Next, each frequency component's contribution to the
transfer function was determined by dividing the input by the
output. As implied in the earlier discussion, using an impulse as
input produces a smooth function in frequency space, contributing
information to the transfer function from all frequency
components. Since the results of the Fourier transforms are
imaginery numbers, their quotient is also imagery, as follows:

$$H(f)^{-1} = \frac{Y(f)}{X(f)} = \frac{(a_1 + b_1 i)}{(a_2 + b_2 i)} = \frac{a_1 a_2 + b_1 + b_2}{a_2^2 + b_2^2} + \frac{(b_1 a - a_1 b_2)}{a_2^2 + b_2^2} i \qquad (7)$$

where $H(f)^{-1}$ is the inverse transfer function;

$Y(f)$ is the transform of the laboratory "impulse";

$Z(f)$ is the transform of the laboratory output;

a_1, a_2 are the real parts of the input and output
transforms;

b_1, b_2 are the imaginary parts of the input and output
transforms.

The experimental time series (measured output) is then transformed, and multiplied by the inverse transfer function to yield the input waveform,

$$U(f) = X(f)H(f)^{-1} = \frac{a_1 a_2 a_3 + b_1 b_2 a_3}{a_2^2 + b_2^2} - \frac{b_1 a_2 b_3 - a_1 b_2 b_3}{a_2^2 + b_2^2} +$$

$$\left[\frac{a_1 a_2 b_3 + b_1 b_2 b_3}{a_2^2 + b_2^2} + \frac{b_1 a_2 a_3 - a_1 b_2 a_3}{a_2^2 + b_2^2} \right] i \qquad (8)$$

where $U(f)$ is the tranform of "true" input waveform;

$X(f)$ is the transform of measured output waveform;

a_3 is the real part of the output transform;

b_3 is the imaginary part of the output transform.

Finally, an inverse transform yields the "true" input time series.

XFORM next called the DELAY and ROTATE subroutines. These subroutines operated on the coordinates of the pass; therefore, when no navigation information was available, they were not used. The DELAY subroutine applied a constant time delay, translated as a shift in the coordinates, to account for the lag time created by system dynamics. This lag time was obtained daily in situ tests. The ROTATE subroutine corrected the concentrations to produce values appropriate to a pass perpendicular to the mean wind direction. In almost all cases, this correction proved to be negligible, since the flight paths were usually within 5 degrees of the desired direction.

The two resultant mass storage data sets were called AIR4 (untransformed passes) and AIR5 (transformed passes). Figures 5 and 6 show two examples of untransformed and transformed data. The abscissa represents distance from first detection of SF_6. The apparent change in the peak location upon transformation results from the inherent time shift due to the "smoothing" of the input waveform. In Figure 5, the plume has been significantly narrowed, and the mass conserved with an increase in peak concentration. Also, a second mode appears which corresponds to a slight inflection in the untransformed data. This demonstrates the usefulness of the transfer function approach for retrieving high-frequency information. Figure 6 displays a much broader plume than in Figure 5. The transformation does not significantly change this waveform shape. Evidently, the transformed plume contains significant terms only at frequencies below those affected by the transfer function. Also note that the peak shift remains, since time shifting translates to phase shifting in frequency space, affecting all frequencies.
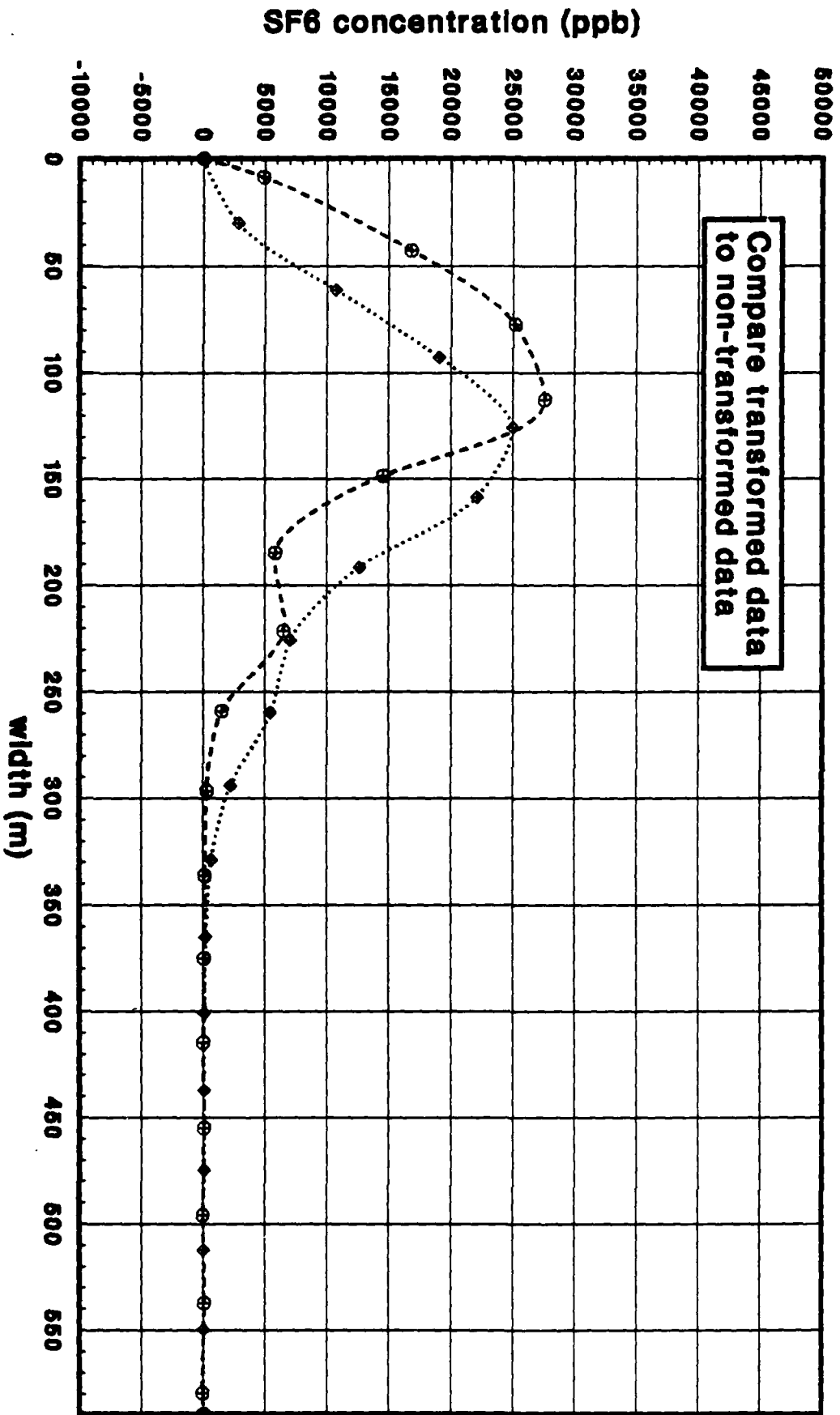
FIGURE 5. EXAMPLE OF ANALYSIS STEP 2 OUTPUT (NARROW PLUME)

date : 6/28 time : 15 3: 4 pass 43

SF6 concentration (ppb)

Compare transformed data
to non-transformed data

width (m)

- untransformed
- transformed
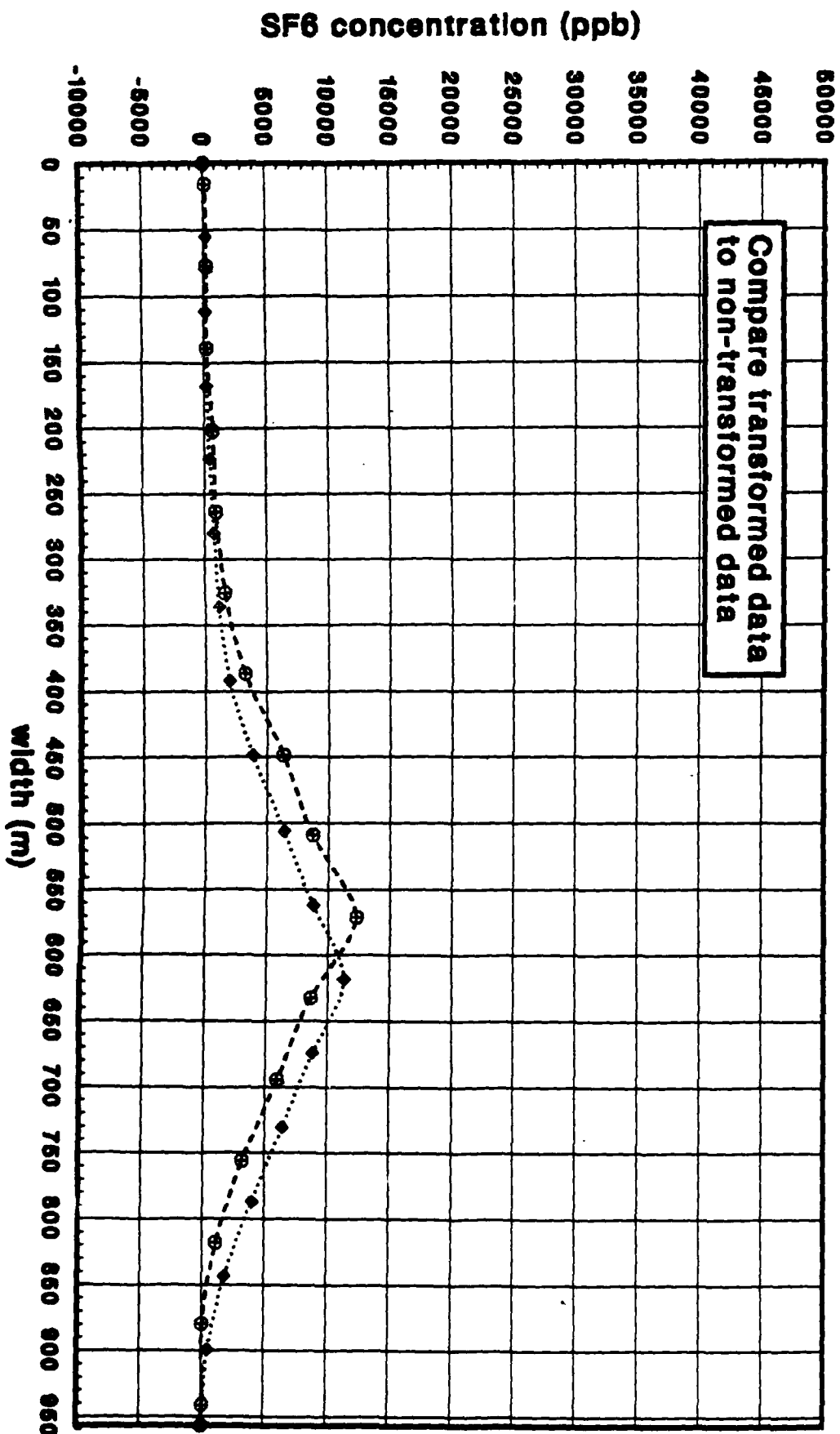
FIGURE 6. EXAMPLE OF ANALYSIS STEP 2 OUTPUT (WIDE PLUME)

Step 3 - Missing Mini-Ranger Data

As mentioned in step one, at times during the experiment one or both mini-ranger signals were not available. Anticipating this problem, various reference points were selected as starting points for plume transects, and the time of intersection logged on the SF6 analyzer strip chart by an onboard technician. With this information, the flight heading, and airspeed, the plume coordinates could be estimated.

The program MINIFIX was written to do the necessary analysis. The heart of this program is a look-up table that lists passes with missing coordinates, and their associated reference point to plume peak distances. These distances were manually extracted from the SF_6 analyzer strip charts. Another table identifies the reference points for the various passes. These reference points are shown in Figure 2 and their positions listed in Table 3.

Since the reference point passage was logged instantaneously and the strip chart data was output by the analyzer, the inherent lag due to the system dynamics (mentioned in the previous section) had to be removed by MINIFIX. Care was taken to operate on the untransformed plume when applying this correction, to avoid the time-shift due to the transformation process.

As in the previous section, the plume was rotated to a wind direction perpendicular alignment. The untransformed and transformed data sets were output to mass storage files AIR6 and AIR7 respectively. Table 4 lists all SF6 cross-sections archived at

24

NPS, and also identifies those passes with missing mini-ranger data. An example of the data sets, AIR4 - AIR7 (identical formats) is presented in Figure 7.

Table 4

Pass Numbers for Which Plume Cross Sections Were Determined*

(complete analysis through the "Missing Mini-Ranger" Step)

DATE (June 82)

21		22		24		25		27		28		29	
54m		4m	58 m	1	41	1	36	1	42	1	67	1	56
55m		5m	59 m	2	42	2	37	2	43	3	68	2	57
56m		6m	62 m	3m	43	3	38		44	4		3	58
8m	57m	7m	63 m		45	4	39	4	46	6	71	4	59
9m	59m	8m	64 m	7	46	6	41	5	47	9	72	5	
	62m	11m	65 m	8	47	7	42	7	48	11	73	7	
11m	63m	12m	34 m	9	48	8	43	8	49	13	74	12	
13m	64m	13m	42 m	10	49	9	44	9	50	15	77	14	19m
14m	65m	14m	3 m	12	53	10	45		51		78	18	22m
15m		15m	26m	13	54	11	46	11	52	17		23	24m
17m	68m	16m	27m	14	55	12	48	14	53	19		27	
19m	72m	17m	30m	15	56	13	49	16		22		29	26m
21m		18m	32m	16	57	14	50	17		26		31t	
23m	75m	19m	6 1m	17	59	15	51	18		27	18m	32	
27m	16m	21m	35m	18	61	16	52	19			21m	33	
28m	18m	22m	36m	19	62	17	53	22		29	23m		
30m	25m	23m	37m	21	63	19	54	24		30	53m	55	
32m	29m	25m		22	64	21	55	25		33	55m	37	
34m	31m	29m		23	66	22	58	26		34			
36m	33m	31m		24	70	23	59	27		35	77m	39	
37m	35m	33m		25	72	24	61	28		37	36	41m	
38m	39m	41m		26	73	25		29				42	
41m	42m	45m		28	74	26	63	30		44		43m	
43m	58m	49m		29	75	27	64	31		46		44	
	61m			30	76	28	65	32		48		45	
45m	69m	51m		31	77	29	66	33		54		46m	
46m	71m	52m		32	80	30	67	34		59		47	
47m	73m	53m		33	81	31	68	35		60		48	
48m	5m	54m		36			61	50					
49m		55m		37		33	70	37		62		51	
	44m	56m		38		34	73	39		65		52	
53m		57m		39		35	57m	41		66		55	

pass numbers

* stored at NPS computer center as "AIR6" (untransformed), and "AIR7" (transformed)
m mini-ranger not operating during this pass
t this pass represented as two logical records

26

Figure 7.

EXAMPLE OF ANALYSIS STEPS 2,3 OUTPUTS

FILE: [illegible]   [illegible]   NAVAL POSTGRADUATE SCHOOL

[illegible data output — faded/unreadable tabular data]

:
:

INDIVIDUAL LINE KEY:

line 1: time in PST, pass numbers start at the beginning
of each experimental day

3: DWD is downwind distance from the source

6-: data -each profile has been time center averaged
to 18 points
-SF6 is concentration in PPT
-all lengths are in meters

27

Step 4 - Multi-modal Gaussian Fits

In plume dispersion modelling, mass distributions are most often described by the familiar Gaussian, or normal, distribution on the horizontal plane. To parameterize these models, then, the measured plume cross-sections must also be approximated in a similar fashion.

The success with which a Gaussian shape approximates the actual measured cross-wind profiles will, of course, vary a great deal. Cross-sections were often skewed, multi-modal, or "square-shaped". This analysis step started by determining the standard deviation of the mass from the mean position. In discrete form,

$$\sigma_y = \sqrt{\frac{N(C-B^2)}{N-1}} \qquad (9)$$

$$C = \frac{1}{T} \sum_{i=1}^{N} f(x_i)(x_i - x_1)^2 \qquad (10)$$

$$B = \frac{1}{T} \sum_{i=1}^{N} f(x_i)(x_i - x_1) \qquad (11)$$

$$T = \sum_{i=1}^{N} f(x_i) \qquad (12)$$

where N   is total number of points;

$f(x_i)$ is mass, or concentration, at the ith point;

x_i is the cross-wind position of the ith point;

These calculations were performed on both the transformed and untransformed profiles of the previous step. As expected, the transformed width was always smaller than the untransformed value, due to the "peak sharpening" effect of the transfer function.

The next task performed in this analysis was a numerical curve fit to the multi-modal Gaussian model, defined as follows:

$$f(y) = \sum_{i-1}^{n} P_i \exp\left[\frac{-(y-\mu_i)^2}{2\sigma_i^2}\right] \tag{13}$$

where n   is the total number of modes;

    μ_i is the cross-wind position of the i th   mode;

    $f(y)$ is the model value at position x;

    P_i is the peak concentration of the i th   mode;

    σ_i^2 is the variance of the i th   mode.

Because no unique solution to this curve fitting exists, the program required interactive decisions for each profile. The user initially decided on the number and cross-wind positions of the modes. The program then selected the concentrations at those positions to be the model's amplitude parameters, and calculated the mode variances necessary to minimize the squared deviations from the fit. The fit and observed profile were then graphically displayed for the user. At this point the user could either accept the fit, or alter his/her initial parameters to achieve a more realistic model. Once satisfied, the user "graded" the profiles subjectively in three categories: skewness, ripple, and overall goodness of fit. Skewness refers to the assymetry of

the individual waveforms associated with each mode. Ripple is the high frequency "noise" introduced to the profiles through the fast Fourier transforms. Goodness of fit judges how well the Gaussian model approximates the observed profile. Table 5 lists the complete set of profiles and grades in each category.

The results from this analysis step are stored in the mass storage data set AIR8. An example of AIR8 is supplied in Figure 8. Examples of observed profiles and their associated analytical forms is shown in Figures 9-12. Figure 9 demonstrates a reasonably well-behaved profile. Figure 10 shows a bimodal distribution. The Figures 10 and 11 data hint at an additional mode in the distribution; however, the programmer decided to ignore the minor peak. Some subjectivity was inevitable in this analysis step. The high frequency components in Figure 12, however, are ripple, produced in the FFT. In this case, the model profile is probably closer to reality than the transformed data.

Table 5

Subjectively Determined Quality Analysis

of Multi-Modal Gaussian Fits

to SF6 Cross-Sections

1. Grading System

GRADE

Test	U	A	B	C	Y	N
Ripple	--	negligible	amplitude of ripple less than 20% of peak	amplitude of ripple greater than 20% of peak	--	--
Skewness	Undetermined because of waveform overlap	less than 20% of mass displaced	20-50% of mass displaced	greater than 50% of mass displaced	--	--
Goodness of fit	--	maximum deviation less than 20%	maximum deviation 20-50%	maximum deviation greater than 50%	--	--
Aligned	--	--	--	--	model mode aligned with data mode	model mode aligned with data mode

2. Subscripts

+ identifies a fourth mode
** this pass from "AIR7" is deleted because maximum concentration is less than 1000 ppt.

Pass #	ripple	skewness			goodness of fit			aligned		
		peak 1	peak 2	peak 3	peak 1	peak 2	peak 3	peak 1	peak 2	peak 3
5	A	U	U	U	A	A	C	Y	Y	Y
8	C	C	C	--	C	C	--	Y	--	--
9	C	B	--	--	C	--	--	Y	--	--
11	B	B	--	--	B	--	--	Y	--	--
13	B	B	--	--	B	--	--	Y	--	--
14	C	C	--	--	C	--	--	N	--	--
15	A	B	A	--	B	B	--	Y	Y	--
16	C	C	C	--	C	C	--	Y	N	--
17	C	B	--	--	B	--	--	Y	--	--
18	B	A	--	--	A	--	--	Y	--	--
19**
21	C	C	--	--	C	--	--	Y	--	--
23	C	C	--	--	C	--	--	N	--	--
25	C	C	C	--	A	A	--	Y	Y	--
27	A	B	--	--	A	--	--	Y	--	--
28	B	B	--	--	B	--	--	Y	--	--
29	C	C	C	--	B	C	--	Y	Y	--
30	B	B	--	--	A	--	--	Y	--	--
31	C	U	U	U	A	B	A	Y	Y	Y
32	B	C	--	--	C	--	--	Y	--	--
33	B	U	U	U	A	A	A	Y	Y	Y
34	B	C	--	--	C	--	--	Y	--	--
35	B	U	U	U	C	B	B	Y	Y	Y
36	B	C	--	--	B	--	--	Y	--	--
37	A	C	--	--	B	--	--	N	--	--
38	B	C	--	--	A	--	--	Y	--	--
39	B	U	U	--	C	C	--	Y	Y	--
41	B	C	--	--	B	--	--	Y	--	--
42	B	U	U	U,U+	A	A	A,A+	Y	Y	Y,Y+
43	B	B	C	--	B	C	--	Y	Y	--
44	B	U	U	--	B	B	--	Y	Y	--
45	B	C	--	--	C	--	--	Y	--	--
46	A	A	C	--	C	C	--	Y	Y	--
47	A	A	--	--	A	--	--	Y	--	--
48	A	C	C	--	C	B	-	Y	Y	--
49	B	C	--	--	B	--	--	N	--	--
53	A	C	--	--	C	--	--	N	--	--<
54	A	U	U	U	C	A	A	N	N	Y
55	B	C	--	--	B	--	--	N	--	--
56**
57	A	C	--	--	C	--	--	Y	--	--
58	B	U	U	U	C	A	A	Y	Y	N
59	A	C	--	--	B	--	--	Y	--	--
61	B	U	U	U	A	A	C	Y	Y	Y
62	A	C	--	--	B	--	--	N	--	--

Pass #	ripple	skewness			goodness of fit			aligned		
		peak 1	peak 2	peak 3	peak 1	peak 2	peak 3	peak 1	peak 2	peak 3
63	B	C	--	--	B	--	--	Y	--	--
64	A	C	--	--	B	--	--	M	--	--
65	A	C	--	--	B	--	--	N	--	--
68	A	C	C	--	B	B	--	N	Y	--
69	C	C	--	--	B	--	--	Y	--	--
71	B	B	--	--	B	--	--	N	--	--
72	A	B	--	--	B	--	--	Y	--	--
73	B	C	--	--	A	--	--	N	--	--
75	A	U	U	B	B	B	B	Y	Y	N

		skewness			goodness of fit			aligned		
Pass #	ripple	peak 1	peak 2	peak 3	peak 1	peak 2	peak 3	peak 1	peak 2	peak 3
3	B	C	C	--	A	A	--	Y	Y	--
4	C	C	C	--	C	C	--	N	N	--
5	A	B	B	--	C	A	--	N	Y	--
6	A	B	--	--	A	--	--	N	--	--
7	C	C	C	--	A	A	--	Y	Y	--
8	C	C	C	--	C	A	--	Y	Y	--
11	A	C	--	--	A	--	--	Y	--	--
12	A	C	--	--	A	--	--	Y	--	--
13	C	C	C	--	C	C	--	N	N	--
14	B	C	C	--	C	C	--	Y	Y	--
15	A	C	--	--	C	--	--	N	--	--
16	A	B	--	--	A	--	--	Y	--	--
17	C	B	--	--	C	--	--	Y	--	--
18	C	C	--	--	B	--	--	Y	--	--
19	B	C	C	--	B	A	--	Y	Y	--
21	A	C	--	--	A	--	--	Y	--	--
22	B	C	--	--	A	--	--	Y	--	--
23	A	B	--	--	C	--	--	Y	--	--
25	C	C	--	--	C	--	--	--	--	--
26	C	C	--	--	C	--	--	N	--	--
27	C	U	U	U	A	A	A	Y	Y	Y
29	**
30	A	U	U	U	B	A	A	Y	Y	Y
31	C	C	--	--	C	--	--	Y	--	--
32	A	U	U	U	A	A	A	Y	Y	Y
33	C	B	C	--	B	C	--	Y	N	--
34	A	B	--	--	A	--	--	N	--	--
35	B	B	--	--	B	--	--	N	--	--
36	A	C	--	--	A	--	--	Y	--	--
37	B	C	C	--	A	C	--	Y	Y	--
41	B	C	C	C	B	C	B	Y	N	N
42	A	C	--	--	A	--	--	Y	--	--
45	B	C	C	--	B	B	--	Y	Y	--
49	C	C	C	C	B	B	B	Y	Y	Y
51	B	U	U	--	C	B	--	Y	Y	--
52	A	U	U	--	B	A	--	Y	Y	--
53	A	C	C	--	B	A	--	N	N	--
54	A	A	--	--	A	--	--	Y	--	--
55	A	B	B	--	A	A	--	Y	Y	--
56	A	C	B	--	C	A	--	Y	N	--
57	C	U	U	--	A	C	--	N	Y	--
58	A	C	--	--	A	--	--	N	--	--
59	A	U	U	U	A	A	A	Y	Y	Y
61	A	U	U	U,U+	B	B	C,C+	Y	N	N,N+
62	A	U	U	U	A	A	B	Y	Y	N
63	B	C	C	--	A	A	--	Y	Y	--
64	A	U	U	--	B	B	--	Y	Y	--
65	A	U	U	--	A	A	--	Y	Y	--

Pass #	ripple	skewness			goodness of fit			aligned		
		peak 1	peak 2	peak 3	peak 1	peak 2	peak 3	peak 1	peak 2	peak 3
1	A	C	--	--	C	--	--	Y	--	--
2	B	B	--	--	A	--	--	N	--	--
3	C	C	C	--	B	B	--	Y	Y	--
6	A	A	U	U	A	A	A	Y	Y	Y
7	A	C	--	--	B	--	--	Y	--	--
8	C	C	--	--	C	--	--	Y	--	--
9	A	B	--	--	B	--	--	N	--	--
10	A	B	--	--	C	--	--	N	--	--
12	A	B	--	--	B	--	--	N	--	--
13	A	U	U	--	C	A	--	Y	N	--
14	A	C	--	--	C	--	--	N	--	--
15	B	C	--	--	A	--	--	N	--	--
16	A	A	--	--	A	--	--	Y	--	--
17	A	A	A	--	A	A	--	Y	Y	--
18	B	A	C	--	A	A	--	Y	N	--
19	A	B	--	--	C	--	--	N	--	--
21	B	B	--	--	B	--	--	Y	--	--
22	A	U	U	--	A	B	--	Y	N	--
23	A	B	--	--	C	--	--	Y	--	--
24	**									
25	A	U	U	--	A	A	--	N	Y	--
26	C	A	--	--	C	--	--	Y	--	--
28	A	B	--	--	A	--	--	Y	--	--
29	B	B	--	--	B	--	--	Y	--	--
30	A	C	--	--	C	--	--	Y	--	--
31	B	C	--	--	C	--	--	N	--	--
32	A	C	C	--	B	B	--	Y	Y	--
33	C	A	--	--	C	--	--	Y	--	--
36	A	B	B	--	A	A	--	Y	N	--
37	A	B	--	--	C	--	--	Y	--	--
38	A	C	C	--	B	A	--	Y	Y	--
39	A	A	C	--	A	A	--	Y	Y	--
41	A	C	--	--	A	--	--	Y	--	--
42	**									
43	A	C	A	--	A	A	--	Y	Y	--
45	A	B	--	--	C	--	--	Y	--	--
46	B	A	C	--	A	B	--	Y	Y	--
47	A	B	B	--	B	A	--	Y	Y	--
48	A	A	A	--	A	A	--	Y	Y	--
49	A	C	--	--	C	--	--	Y	--	--
53	A	?	?	--	A	A	--	Y	Y	--
54	A	A	C	--	A	A	--	Y	Y	--
55	A	C	--	--	A	--	--	Y	--	--
56	A	B	B	--	A	A	--	Y	Y	--
57	A	B	A	--	A	A	--	Y	Y	--
59	A	C	B	--	C	B	--	Y	Y	--
61	C	C	C	--	B	C	--	N	Y	--

35

Pass #	ripple	skewness			goodness of fit			aligned		
		peak 1	peak 2	peak 3	peak 1	peak 2	peak 3	peak 1	peak 2	peak 3
62	B	C	--	--	B	--	--	Y	--	--
63	A	C	U	--	A	C	--	Y	Y	--
64	A	A	--	--	C	--	--	Y	--	--
66	A	C	--	--	C	--	--	Y	--	--
70	A	U	U	--	A	A	--	N	Y	--
72	A	C	B	--	C	B	--	Y	Y	--
73	A	C	C	--	A	A	--	Y	Y	--
74	A	A	--	--	A	--	--	Y	--	--
75	A	B	C	--	A	C	--	Y	Y	--
76	B	B	--	--	B	--	--	N	--	--
77	C	A	--	--	C	--	--	Y	--	--
80	A	A	--	--	B	-	--	Y	--	--
81	B	C	--	--	C	--	--	Y	--	--

Pass #	ripple	skewness			goodness of fit			aligned		
		peak 1	peak 2	peak 3	peak 1	peak 2	peak 3	peak 1	peak 2	peak 3
1	A	B	--	--	A	--	--	Y	--	--
2	B	B	--	--	A	--	--	Y	--	--
3	A	B	--	--	A	--	--	Y	--	--
4	C	C	--	--	C	--	--	Y	--	--
6	A	A	--	--	A	--	--	Y	--	--
7	A	B	--	--	A	--	--	N	--	--
8	A	C	--	--	A	--	--	Y	--	--
9	A	B	--	--	A	--	--	Y	--	--
10	A	C	--	--	A	--	--	N	--	--
11	A	B	--	--	C	--	--	Y	--	--
12	B	C	--	--	C	--	--	Y	--	--
13	A	U	U	--	A	A	--	Y	Y	--
14	A	C	--	--	C	--	--	N	--	--
15	A	C	--	--	C	--	--	N	--	--
16	**									
17	A	C	C	--	C	C	--	Y	--	--
19	A	B	--	--	A	--	--	N	--	--
21	B	C	--	--	C	--	--	Y	--	--
22	A	C	--	--	B	--	--	N	--	--
23	A	C	--	--	C	--	--	Y	--	--
24	A	B	--	--	A	--	--	N	--	--
25	C	C	--	--	C	--	--	N	--	--
26	C	C	--	--	A	--	--	N	--	--
27	B	C	C	--	A	A	--	N	N	--
28	A	U	U	U	A	A	A	Y	Y	Y
29	A	U	U	--	A	A	--	Y	Y	--
30	A	U	U	U	A	A	A	Y	Y	Y
31	A	C	C	--	C	A	--	Y	N	--
32	A	C	--	--	A	--	--	N	--	--
33	**									
34	B	U	U	U	A	A	A	Y	Y	Y
35	A		--	--	C	--	--	Y	--	--
36	A	B	--	--	B	--	--	N	--	--
37	A	B	--	--	A	--	--	Y	--	--
38	A	A	--	--	A	--	--	Y	--	--
39	A	U	U	--	A	A	--	Y	N	--
41	A	U	U	--	C	A	--	Y	Y	--
42	A	U	U	--	A	A	--	Y	N	--
43	A	B	--	--	A	--	--	N	--	--
44	B	B	--	--	C	--	--	Y	--	--
45	B		B	--	--	C	--	--	Y	--
46	A	C	--	--	A	--	--	Y	--	--
48	A	U	U	--	A	A	--	Y	N	--
49	A	U	U	--	A	A	--	Y	Y	--
50	A	U	U	--	B	B	--	Y	Y	--
51	A	A	--	--	A	--	--	Y	--	--
52	A	U	U	--	A	A	--	Y	Y	--

37

Pass #	ripple	skewness			goodness of fit			aligned		
		peak 1	peak 2	peak 3	peak 1	peak 2	peak 3	peak 1	peak 2	peak 3
53	A	C	C	--	C	A	--	Y	Y	--
54	A	U	U	--	A	A	--	Y	Y	--
55	A	B	--	--	A	--	--	N	--	--
57	***									
58	A	A	--	--	A	--	--	Y	--	--
59	B	B	A	--	B	A	--	Y	Y	--
61	A	C	--	--	A	--	--	Y	--	--
63	A	?	--	--	A	--	--	Y	--	--
64	A	C	C	--	A	A	--	Y	Y	--
65	A	B	--	--	C	--	--	Y	--	--
66	A	C	--	--	A	--	--	N	--	--
67	A	A	A	--	B	B	--	N	Y	--
68	C	C	--	--	C	--	--	N	--	--
69	A	B	--	--	A	--	--	Y	--	--
70	A	C	--	--	C	--	--	N	--	--
73	A	B	--	--	B	--	--	Y	--	--

Pass #	ripple	skewness			goodness of fit			aligned		
		peak 1	peak 2	peak 3	peak 1	peak 2	peak 3	peak 1	peak 2	peak 3
1	A	B	--	--	A	--	--	Y	--	--
2	C	C	--	--	B	--	--	N	--	--
4	A	B	--	--	A	--	--	Y	--	--
5	A	B	--	--	A	--	--	N	--	--
7	A	C	--	--	A	--	--	N	--	--
8	**									
9	A	B	--	--	A	--	--	N	--	--
11	A	B	--	--	A	--	--	Y	--	--
14	A	C	--	--	A	--	--	N	--	--
16	B	B	--	--	B	--	--	Y	--	--
17	A	B	--	--	A	--	--	Y	--	--
18	C	B	--	--	B	--	--	N	--	--
19	A	B	--	--	A	--	--	Y	--	--
22	A	B	--	--	A	--	--	Y	--	--
24	A	B	--	--	A	--	--	N	--	--
25	C	C	C	--	C	C	--	Y	Y	--
26	A	B	--	--	A	--	--	Y	--	--
27	B	C	C	--	A	C	--	Y	N	--
28	A	B	--	--	A	--	--	Y	--	--
29	A	C	--	--	C	--	--	N	--	--
30	A	C	--	--	C	--	--	N	--	--
31	A	A	--	--	A	--	--	Y	--	--
32	A	B	--	--	Y	--	--	N	--	--
33	A	B	--	--	A	--	--	Y	--	--
34	A	U	U	--	A	A	--	Y	Y	--
35	A	U	U	--	A	A	--	N	Y	--
36	A	C	--	--	A	--	--	N	--	--
37	C	C	--	--	C	--	--	Y	--	--
39	A	A	--	--	A	--	--	Y	--	--
41	A	B	--	--	A	--	--	Y	--	--
42	A	B	--	--	A	--	--	Y	--	--
46	A	B	C	--	A	A	--	Y	Y	--
47	A	B	--	--	Y	--	--	N	--	--
48	B	C	--	--	C	--	--	N	--	--
49	A	B	--	--	A	--	--	N	--	--
51	A	B	--	--	A	--	--	Y	--	--
52	A	C	--	--	C	--	--	Y	--	--
53	A	B	--	--	A	--	--	Y	--	--
43	**									
44	**									

		skewness			goodness of fit			aligned		
Pass #	ripple	peak 1	peak 2	peak 3	peak 1	peak 2	peak 3	peak 1	peak 2	peak 3
1	A	C	--	--	C	--	--	N	--	--
3	B	B	--	--	A	--	--	N	--	--
4	A	C	--	--	B	--	--	N	--	--
6	C	C	C	--	A	A	--	Y	Y	--
9	B	B	--	--	C	--	--	Y	--	--
11	A	C	--	--	A	--	--	N	--	--
13	A	C	--	--	A	--	--	Y	--	--
15	A	C	C	C	A	A	A	Y	Y	Y
17***										
18	A	C	--	--	A	--	--	Y	--	--
19	A	C	--	--	A	--	--	N	--	--
21	A	C	--	--	A	--	--	Y	--	--
22***										
23***										
26	B	B	--	--	C	--	--	Y	--	--
27	A	C	--	--	B	--	--	Y	--	--
29	A	A	A	--	A	A	--	Y	Y	--
30***										
33	C	C	--	--	C	--	--	Y	--	--
34	A	A	--	--	A	--	--	Y	--	--
35	A	C	--	--	C	--	--	Y	--	--
36	A	C	--	--	A	--	--	N	--	--
37	B	C	C	--	B	B	--	Y	Y	--
44	A	C	A	--	A	A	--	Y	N	--
46	A	B	--	--	A	--	--	Y	--	--
48	A	C	--	--	A	--	--	N	--	--
53	A	C	--	--	B	--	--	N	--	--
54	A	C	--	--	B	--	--	N	--	--
55	A	B	--	--	A	--	--	Y	--	--
59	A	B	--	--	C	--	--	Y	--	--
60	A	B	--	--	A	--	--	Y	--	--
61	A	B	C	--	A	A	--	Y	Y	--
62	B	C	--	--	C	--	--	Y	--	--
65	B	C	--	--	B	--	--	Y	--	--
66	B	B	--	--	A	--	--	Y	--	--
67	A	C	--	--	A	--	--	Y	--	--
68	A	C	C	--	A	A	--	Y	Y	--
71	A			--	B	B	--	N	N	--
72	A	C	--	--	C	--	--	N	--	--
73	A				A	A	A	N	Y	Y
74	A	B	--	--	A	--	--	Y	-	--
77	C	C	C	C,C+	A	A	A,A+	Y	Y	Y,Y+
78	A	C	--	--	A	--	--	Y	--	--

Pass #	ripple	skewness			goodness of fit			aligned		
		peak 1	peak 2	peak 3	peak 1	peak 2	peak 3	peak 1	peak 2	peak 3
1	B	C	--	--	C	----	--	Y	--	--
2	A	U	U	--	A	C	--	Y	Y	--
3	B	C	--	--	B	--	--	Y	--	--
4	B	B	--	--	C	--	--	Y	--	--
5	A	B	--	--	C	--	--	Y	--	--
7	B	C	--	--	C	--	--	N	--	--
12	A	C	--	--	C	--	--	Y	--	--
14	B	C	--	--	C	--	--	Y	--	--
18	A	B	--	--	A	--	--	Y	--	--
19	D	C	--	--	C	--	--	Y	--	--
22	***									
23	A	C	--	--	C	--	--	Y	--	--
24	A	C	--	--	C	--	--	Y	--	--
26	A	U	U	--	A	A	--	N	N	--
27	A	C	--	--	C	--	--	Y	--	--
29	A	C	--	--	A	--	--	Y	--	--
31	A	C	C	A	A	C	A	Y	Y	Y
32	A	B	--	--	A	--	--	N	--	--
33	B	C	--	--	B	--	-	Y	--	--
35	C	C	--	--	C	--	--	Y	--	--
37	A	B	--	--	A	--	--	Y	--	--
39	A	B	--	--	A	--	--	Y	--	--
41	A	C	B	--	A	A	--	Y	N	--
42	A	B	--	--	C	--	--	Y	--	--
43	A	A	--	--	A	--	--	Y	--	--
44	B	B	B	B	B	C	B	Y	Y	Y
45	C	C	--	--	C	--	--	Y	--	--
46	A	B	--	--	A	--	--	Y	--	--
47	B	C	--	--	C	--	--	Y	--	--
48	B	C	--	--	C	--	--	Y	--	--
50	B	C	--	--	C	--	--	Y	--	--
51	B	B	--	--	A	--	--	Y	--	--
52	B	C	--	--	A	--	--	Y	--	--
53	A	C	U	U	C	B	A	Y	Y	N
56	B	C	C	--	A	B	--	Y	Y	--
58	B	C	C	--	A	A	--	Y	N	--
60	A	U	U	U	A	A	A	Y	Y	Y

41

Figure 8.

EXAMPLE OF ANALYSIS STEP 4 OUTPUT

INDIVIDUAL LINE KEY:

line 1: DIR is flight heading in degrees
   2: DWD is downwind distance from source
   3: XO,YO are coordinates of plume where "width"
      has a value of zero
   4: total pass mean is in relation to "width" in
      the direction of the flight heading
   8: waveforms refer to the individual modes of the
      Gaussian fit
   9: peak value is in PPT

42

date : 6/25 time : 1217:11 pass 11
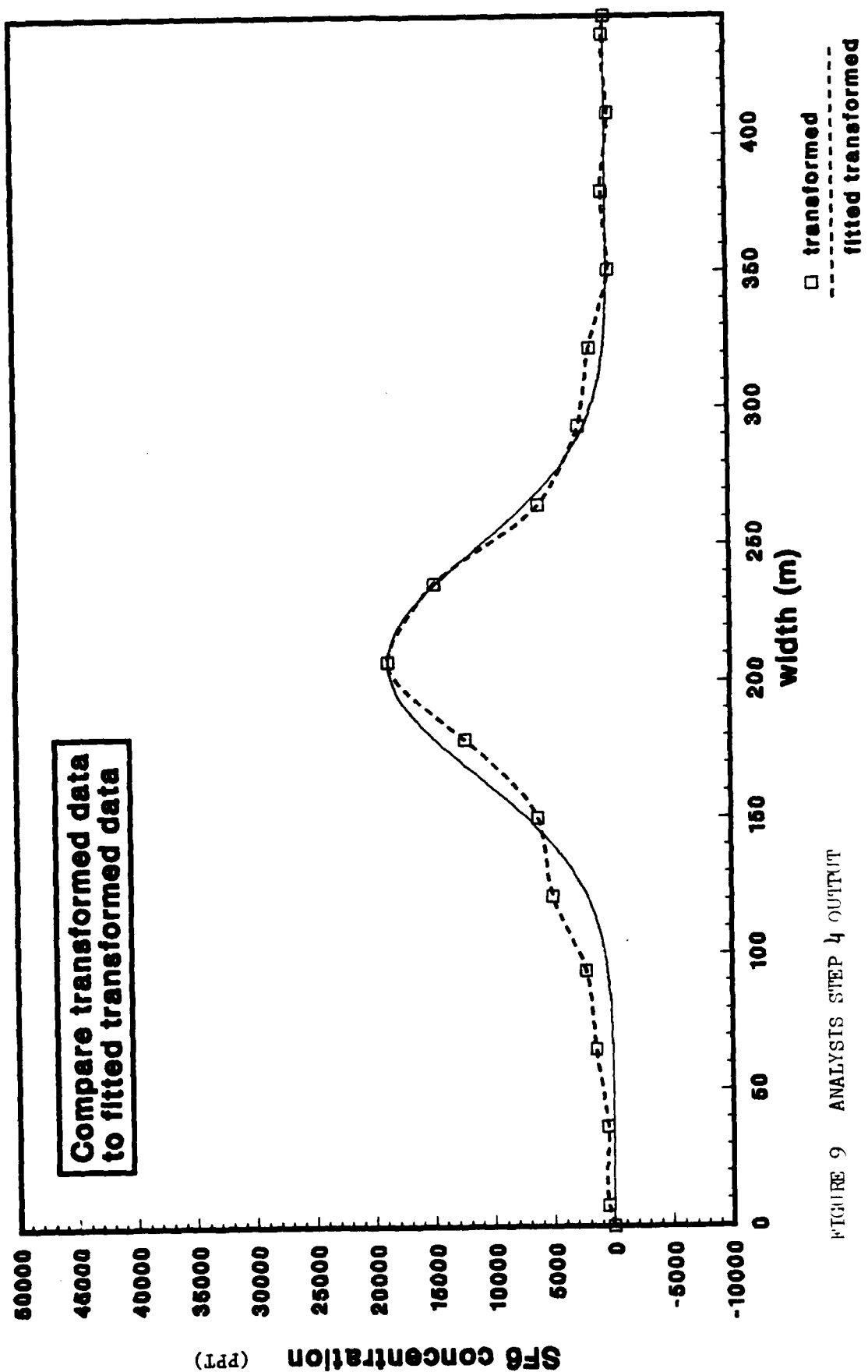
Compare transformed data
to fitted transformed data

□ transformed
--- fitted transformed

width (m)

SF6 concentration (ppt)

FIGURE 9   ANALYSIS STEP 4 OUTPUT

date : 6/22 time : 1536:22 pass 19

Compare transformed data
to fitted transformed data

□ transformed
---- fitted transformed

FIGURE 10   ANALYSIS STEP : OUTPUT

SF6 concentration (PPT)

width (m)

date : 6/28 time : 1415:49 pass 27
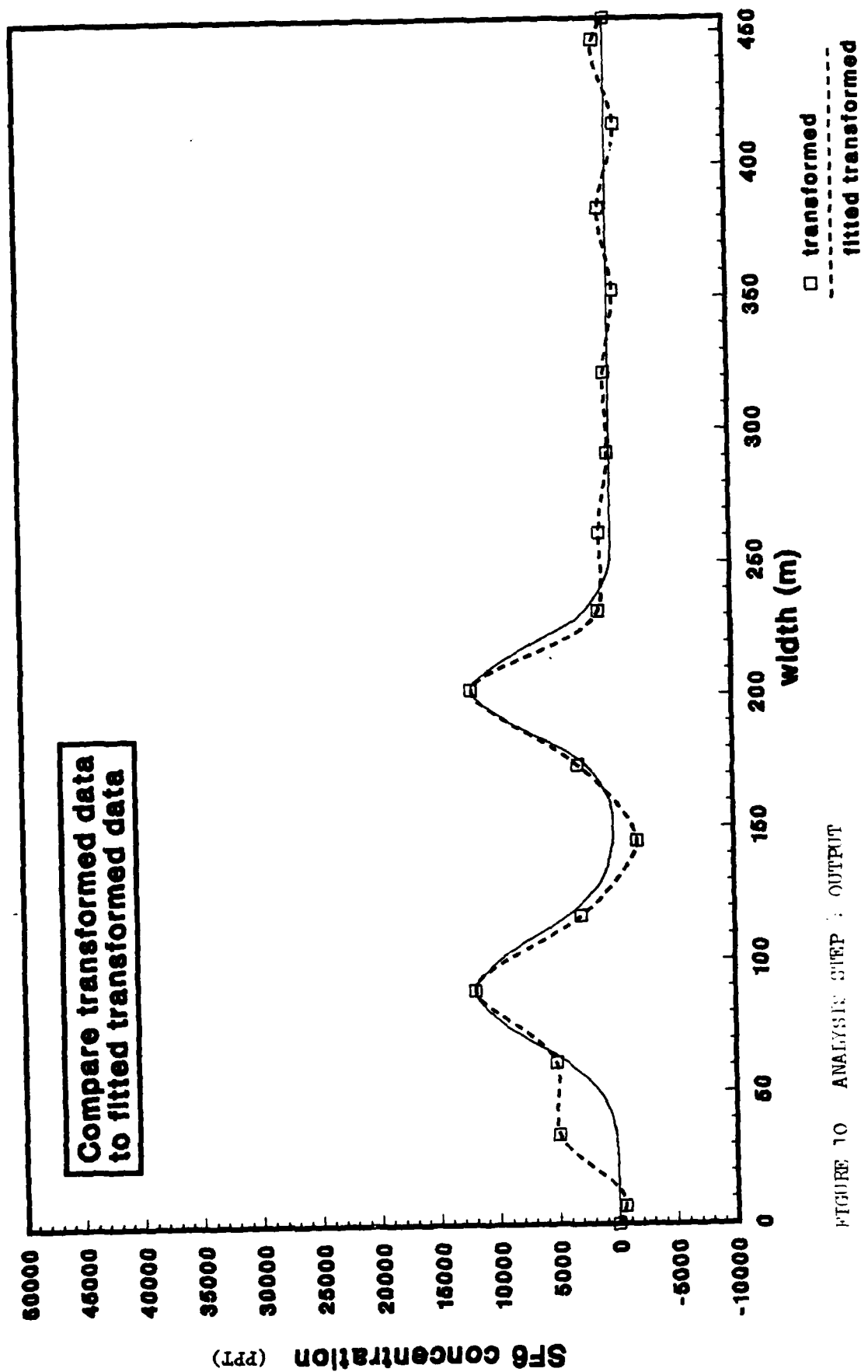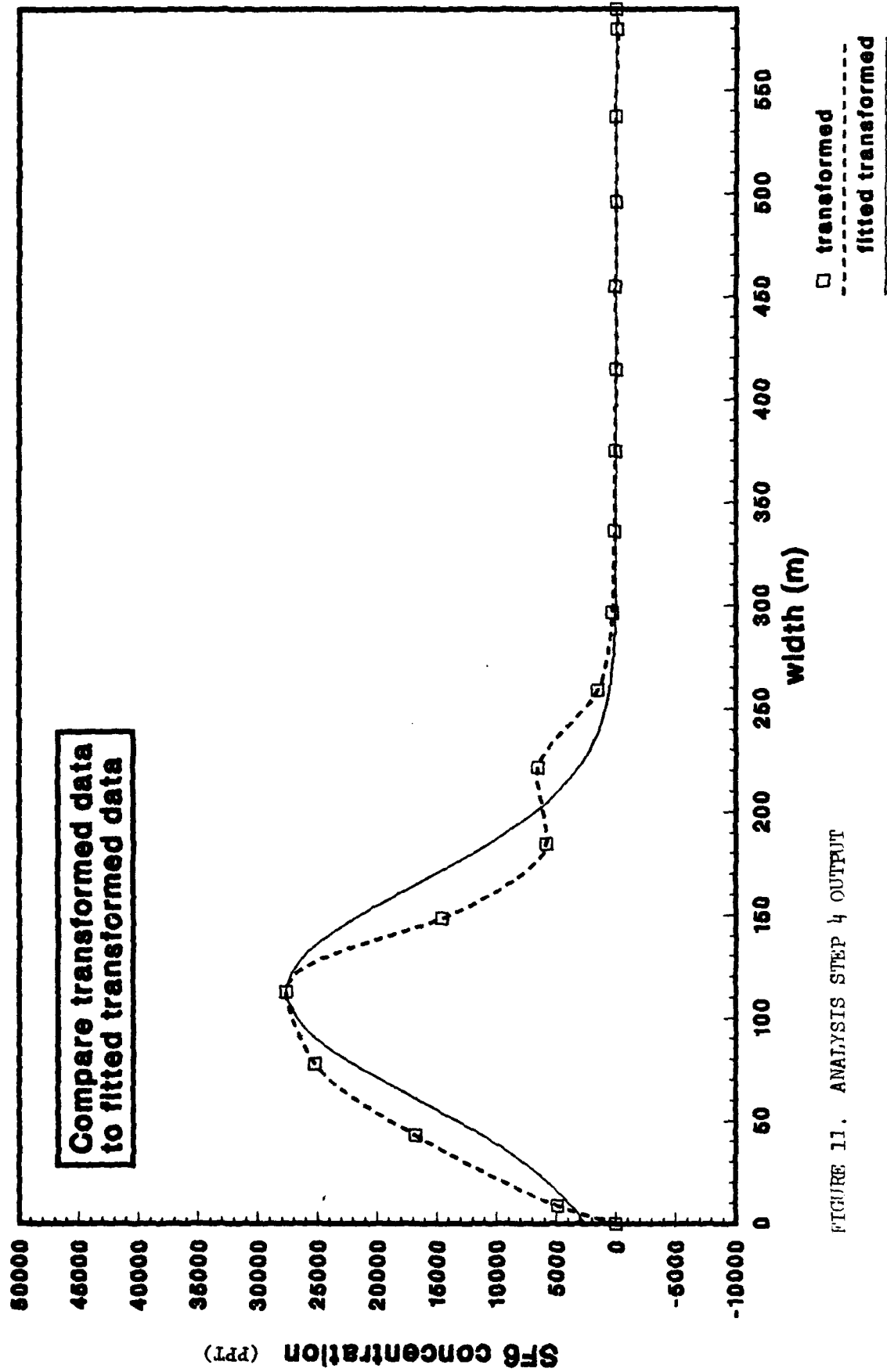
FIGURE 11. ANALYSIS STEP 4 OUTPUT

date : 6/25 time : 1147:30 pass 2

Compare transformed data
to fitted transformed data

□ transformed
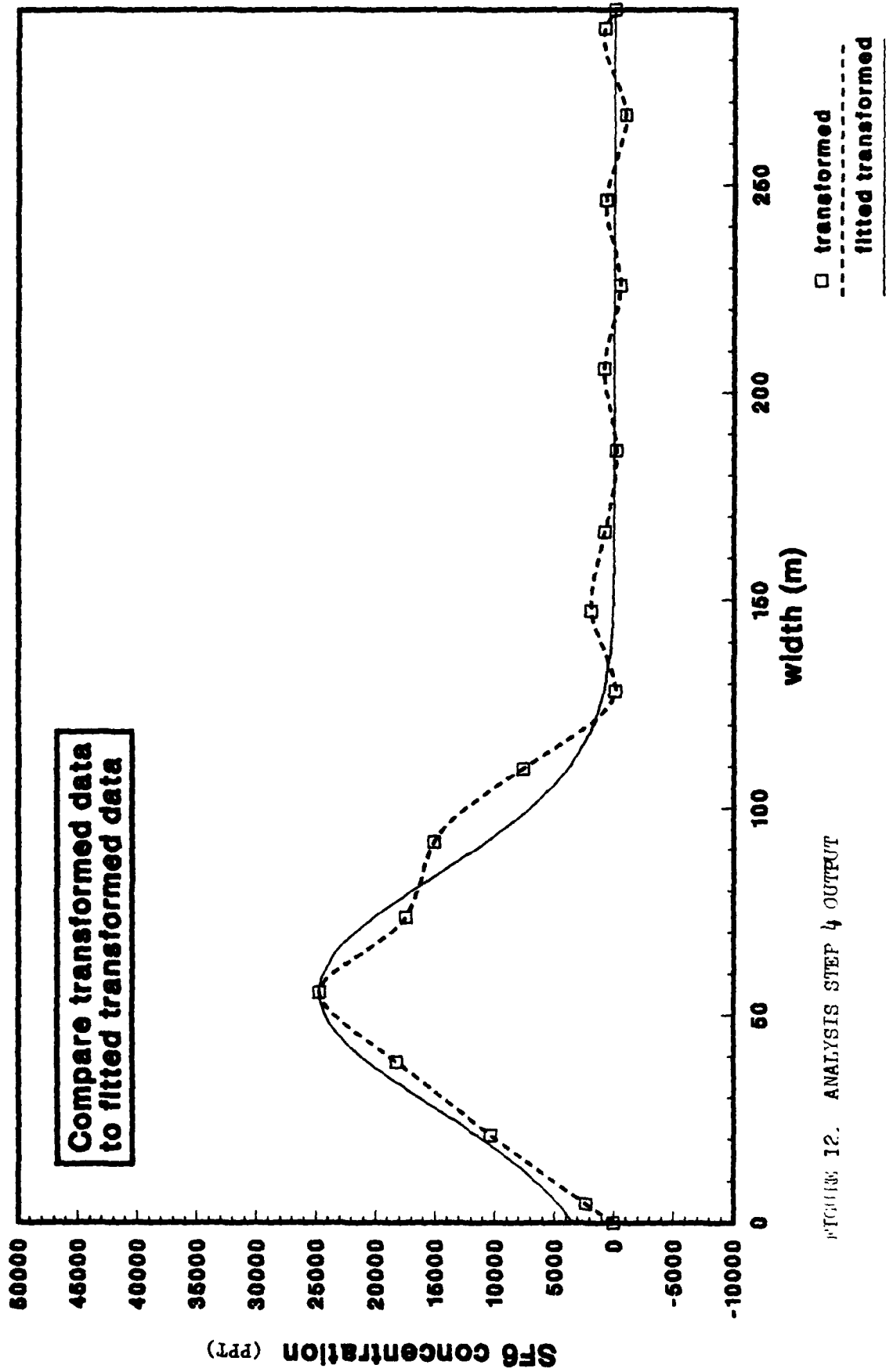--- fitted transformed

width (m)

SF6 concentration (ppt)

FIGURE 12. ANALYSIS STEP 4 OUTPUT

Step 5 - Calculation of Hourly Averages

Many dispersion models attempt to predict concentrations expected when averaged over a one-hour period. In order to relate the results of this data set to those of the past, and also in order to satisfy contractual agreements, this analysis step formed one-hour averages of the horizontal and vertical plume growth parameters, σ_y and σ_z. In addition, this step added a header to the data set containing a variety of averaged meteorlogical quantities.

The basic procedure in this step was to read in half-hour average met data twice, form one-hour average met data, read in tracer data for the current hour, bin the tracer profiles according to range from the release point, and perform the averaging calculations for the plume.

The meteorological data was described in Schacher et al. (1982) and was exclusively collected at the release platform. To account for plume flight-time from the platform, a lag of one-half hour was applied when synchronizing the two-data sets. Even with this adjustment, many problems exist in determining the appropriate meteorology. Due to spatial inhomogeneity, meteorological conditions at the platform become less representative of the average met conditions experienced by the plume as the downwind distance to the aircraft transects increase. Also, meteorological averages tend to differ significantly from hour to hour, implying that stationarity through the one-hour period may be a weak assumption.

47

For each experimentation day, four range bins were selected, based on the distribution of individual transect downwind distances. An attempt was made to maximize the number of passes in each range bin for all hours, while minimizing the standard deviation of the downwind distances within each range bin. Table 6 lists the range bins for each day.

Table 6

Range Bins for Hourly Averages of Plume Parameters

DAY	BIN 1	BIN 2	BIN 3	BIN 4
	Transect Downwind Distance (m)			
6-21-82	0-1000	1001-2000	2001-3000	3001-4500
6-22-82	0-1000	1001-2000	2001-3000	3001-4000
6-24-82	0-2000	2001-3000	3001-4000	4001-5000
6-25-82	0-2000	2001-3500	3501-5000	unused
6-27-82	0-2000	2001-3500	3501-5000	5001-6500
6-28-82	0-2500	2501-5000	5001-7500	7501-10,000
6-29-82	0-2500	2501-5000	5001-7500	7501-10,000

One major problem in this analysis step was collecting a sufficiently large number of transects for a range bin during a given hour. Typically, this number was 5 to 12 passes per average.

Discussion of the possibilities and consequences of insufficient sampling

will be presented in a later section.

The first averaging calculations performed for each hour-range bin

were the average and standard deviation of the bin's downwind distance.

The downwind distance (DWD) of a cross-section was interpreted as the straight

line distance from the release platform to the plume center. As stated above,

the standard deviations of the DWDs for a range bin was minimized to determined

range bin boundaries. All DWD standard deviations are less than 200 m.

Five different horizontal plume parameters were calculated for each

hour-range bin. Each operated on the ensemble of transects for a bin in a

different way. Table 7 gives symbolic definitions used in the discussion

that follows.

Table 7

Definitions for Horizontal Plume Parameters
Calculated for Each Hour/Range Bin

Symbol	Definition
σ_{yd}	Mean total standard deviations of the horizontal mass distributions from direct calculations.
σ_{yf}	Mean total standard deviations from the uni-modal Gaussian fits.
σ_{yw}	Mean total standard deviations from the uni-modal Gaussian fits weighted by the peak concentration.
σ_{yt}	Mean total standard standard deviations from the uni-modal Gaussian fits averaged in a fixed cross-wind coordinate system.
σ_{ym}	Mean standard deviations from the multi-modal Gaussians fits.

σ_{yd} was the mean of the standard deviations of the horizontal mass distributions as defined in Equations 9-12, operated on the transformed data. The cross-wind coordinate system was allowed to float in this average. In other words, this average is not affected by plume drift.

σ_{yf} is the analytical equivalent of the above. The parameters obtained during the multi-modal Gaussian fits of the previous section were combined to form a single mode fit, and those values averaged. The derivation follows. In continuous form, the mean position of the mass can be defined as the expected value of Y, the "random variable" composed of all y values.

$$E(Y) = {}_{-\infty}\!\int^{+\infty} yF(y)dy \tag{14}$$

where Y   is the "random variable";

        E(Y) is the expected value of Y;

        y   is the cross-wind position;

        F(y) is the density function of y.

The variance is simply the second moment of the distribution, taken about the mean.

$$\sigma_y^2 = E\left[(Y-\mu)^2\right] = E(Y^2) - \mu^2 \tag{15}$$

where μ is the distribution mean; identically E(Y).

In the case of the multi-modal Gaussian model, the mass, or concentration distribution, is described by Equation 13, repeated:

50

$$f(y) = \sum_{i=1}^{n} P_i \exp \left[\frac{-(y-\mu_i)^2}{2\sigma_i^2} \right] \tag{16}$$

where $f(y)$ is the concentration at cross-wind position y,

P_i is the peak concentration of the i th mode.

The density function can be formed by simply normalizing Equation 16 by the integrated mass. The mean, or expected value, of Y is then easily derived as follows:

$$F(y) = \frac{f(y)}{\int_{-\infty}^{+\infty} F(y)\,dy} = \sum_{i=1}^{n} \frac{P_i \exp[-(y-\mu_i)^2/2\sigma_i^2]}{\sum_{j=1}^{n} \sqrt{2\pi}\, \sigma_i P_i} \tag{17a}$$

$$E(y) = \int_{-\infty}^{+\infty} yF(y)\,dy = \sum_{j=1}^{n} \frac{\sigma_j P_j}{\sum_{i=1}^{n} \sigma_i P_i} \int_{-\infty}^{+\infty} \frac{y \exp[-(y-\mu_j)^2/2\sigma_j^2]}{\sqrt{2\pi}\, \sigma_j}\,dy \tag{17b}$$

$$E(y) = \frac{\sum_{i=1}^{n} \sigma_i P_i \mu_i}{\sum_{i=1}^{n} \sigma_i P_i} \tag{17c}$$

Rearranging Equation 15 for the ith mode yields:

$$E_i(Y^2) = \sigma_{yi}^2 + \mu_i^2 \tag{18a}$$

In a similar fashion to the above and using the principle of superposition, it can be shown:

51

$$E(Y^2) = \frac{\sum\limits_{i=1}^{n} \sigma_i P_i (\mu_i^2 + \sigma_i^2)}{\sum\limits_{i=1}^{n} \sigma_i P_i} \qquad (18b)$$

Again using Equation 15, the standard deviation of the ensemble profile with n modes is:

$$\sigma_y = \sqrt{\sigma_y^2} = \sqrt{\frac{\sum\limits_{i=1}^{n} [\sigma_i P_i (\mu_i^2 + \sigma_i^2) - \sigma_i P_i \mu_i]}{\sum\limits_{i=1}^{n} \sigma_i P_i}} \qquad (19)$$

σ_{yf} was obtained by using Equation 19 for each profile, and averaging all values in each hour-range bin. Results were tested by numerically integrating the same profiles and calculating σ_y as in Equations 9-12. Results were within 1%.

σ_{yw} is σ_{yf} weighted by the peak concentration of the member profiles. This parameter is an attempt to bias the mean value toward the cloud width near the plume centroid on the vertical axis, which is ideally at the surface for a surface release. If σ_y is truly independent of height, σ_{yw} should be indentical to σ_{yf}.

σ_{yt} is defined as the mean total standard deviations from the uni-modal Gaussian fits averaged in a fixed coordinate system. σ_{yt} was obtained in identical fashion to σ_{yf} except each transect was fixed in the cross-wind coordinate system before averaging so that the effects of plume centerline drift are included.

σ_{yt} was consistently larger than σ_{yf}. The difference between the values can be interpreted as the degree to which plume meander dominates the hourly averages. In other words, a time-averaged concentration profile can be divided into two components.

Plume spread due to relative diffusion, in which there is no fixed axis, is represented by σ_{yf} mean fit. Henceforth, this will be called the diffusive component, and is often referred to as puff diffusion. It is chiefly influenced by turbulence of length scales close to the size of the cloud. Plume spread due to single particle diffusion relative to a fixed axis is theoretically approached in Taylor's (1921) theorem. Plume growth under this theory is influenced by the integrated energy spectrum, or turbulence of all scales. σ_{yt} is representative of this time-averaged quantity. The difference between σ_{yt} and σ_{yf} fit is the time-averaged plume spread due to turbulence of scales either much larger, or much smaller, than the cloud size. The later contributions are negligible. The former turbulence scales tend to move the whole instantaneous plume in a "snake-like" fashion and will hereafter be referred to as the meander component.

The final horizontal plume parameter calculated was σ_{ym}, the mean standard deviations from the multi-modal fits. This quantity was the mean of all the individual mode widths in a floating coordinate system. The origin of multiple modes in an instantaneous profile is yet unexplained; therefore, the significance of this calculation is unknown. This parameter increases only slowly with range, and may, in fact, define the size of coherent turbulent structures.

53

A parameter calculated during this analysis step closely related to horizontal diffusion was the off-axis position of the mean mass. This is the difference between the actual position of the mean mass and that position calculated from the mean wind vector. The quantity shows any inhomogeniety in the mean wind field, such as a sea breeze's veer with decreasing distance to the shoreline. It also reveals meander produced by motions of time scales longer than the one-hour averaging period.

The vertical standard deviation of the concentration is not measured instantaneously, and therefore must be interpreted from the horizontal cross-sections for each hour-range bin. This was accomplished, when possible, by calculating the cross-wind integrated concentration of each profile, and then performing a single-sided Gaussian fit in the vertical through the data points.

The cross-wind integrated concentration is calculated from the fitted profiles and defined as follows:

$$CWIC_z = \int_{-\infty}^{+\infty} \sum_{i=1}^{n} P_i \exp\left[-(y-\mu_i)^2/2\sigma_{yi}^2\right] dy \qquad (20)$$

$$CWIC_z = \sum_{i=1}^{n} \sqrt{2\pi}\ \sigma_{yi} P_i \qquad (21)$$

54

where $CWIC_z$ is cross-wind integrated concentration in ppt-m at a height z,

σ_{yi} is the standard deviation of the i [th] mode in a given profile,

P_i is the peak concentration of the i [th] mode,

μ_i is the mean position of the i [th] mode.

The model from which σ_z was estimated is:

$$CWIC_z = CWIC_0 \exp \left[- \frac{z^2}{2\sigma_z^2}\right] \tag{22}$$

where σ_z is the vertical standard deviation of mass. By linear regression of $\ln(CWIC_z)$ versus z^2, σ_z becomes a function of only the slope, while $CWIC_0$ is a function of the intercept as follows.

$$\sigma_z = \sqrt{(2a)^{-1}} \tag{23}$$

$$CWIC_0 = \exp(b) \tag{24}$$

where a is the slope of the $\ln(CWIC_z)$ vs z^2 line;

b is the intercept of the line.

Errors in the proposed model presented in Equation 22 can be introduced by either a differing vertical shape of the concentration profile or a non-negligible deposition of SF_6 onto the sea surface. The profile shape was examined by visual inspection of the $\ln(CWIC_z)$ vs z^2 plots. The scatter of the points about the regression line appeared to be unbiased in the vertical for the cases examined, indicating that the $\exp(-z^2)$ model was reasonable.

55

The possibility of mass loss was examined by comparing the ground-level cross-wind integrated concentration predicted by Equation 24 to the value forced by the source emission rate. The Gaussian plume model requires:

$$CWIC_{G*} = \sqrt{\frac{2}{\pi}} \left(\frac{Q}{\sigma_z u}\right) \tag{25}$$

where $CWIC_{G*}$ is ground-level cross-wind integrated concentration predicted by the Gaussian plume model

Q is the emission rate, 25 lb. SF6/hr,

σ_z is the range-dependent vertical plume parameter,

u is the mean wind speed.

Figure 13 shows the ratio of the two values of ground-level cross-wind integrated concentration as a function of range. Ideally, this ratio should be 1 for mass balance. Most points are within a factor of 2. The points are nicely scattered about the identity ratio, and there appears to be no range dependence from 0-9 km.

Based on these results, this analysis suggests that the hourly averaged σ_z values determined by Equation 22 are reasonable.

FIGURE 13

RATIO OF GROUND-LEVEL SF6 MASS CALCULATED
BY REGRESSION TO MASS DERIVED
FROM EMISSION RATE
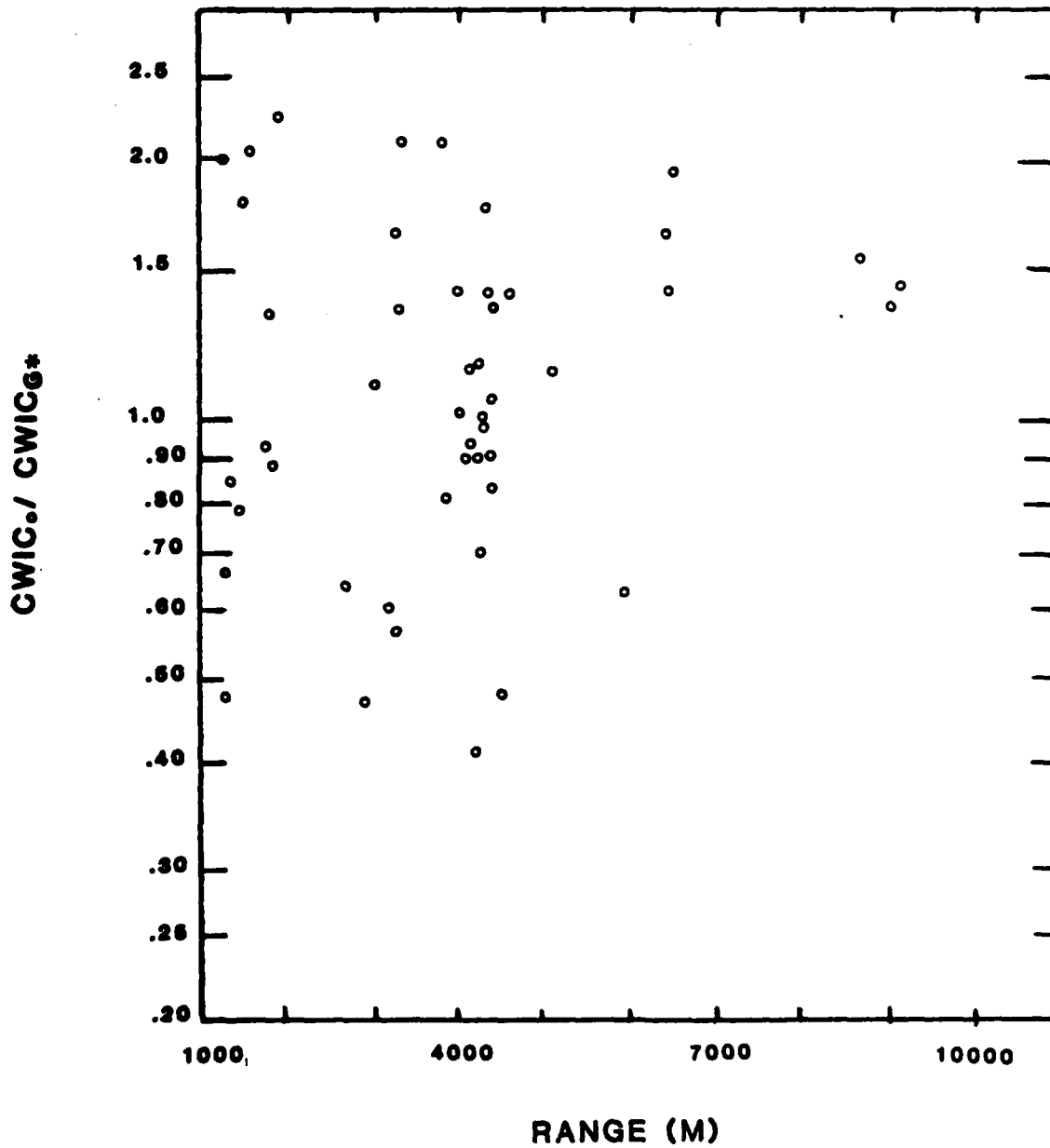
see equation (24-25) for quantity definitions

57

Step 6 - Plume Parameters as a Function
of Range and Stability Class

This analysis step uses the hourly averaged tracer and meteorological data produced in Step 5 to parameterize range-dependent plume growth as a function of commonly obtained shipboard meteorological measurements. This step uses only the fixed fit σ_y in the horizontal plume growth parameterization. Future analysis will concentrate on some of the other forms of the horizontal plume dimension, in order to reduce scatter and examine the effects of averaging time.

This analysis attempts to classify the plume properties on a modification of the well-known Pasquill-Gifford table. (See Gifford [1976]). The original scheme first estimates insolation, based on cloud cover and time of day. Insolation range bin and mean windspeed then determine the appropriate stability class. The scheme essentially makes use of the strong relationship between insolation and buoyancy production of turbulence over land, while relating mean windspeed to mechanical turbulence.

This scheme is not applicable over water because, first of all, buoyancy is only weakly dependent on insolation over the oceans, due to the large specific heat of water. Air-surface temperature differences, the primary factor in buoyant production near the surface, are more often the result of advection of either water or air masses than insolation. Second, while mechanical

58

mixing is still primarily a function of mean windspeed over the
ocean, the analytical form of that relationship is quite
different.

In order to find a common link between dispersion over water
and land, the fundamental physical mechanisms must be examined.
At a given height, dispersion is primarily a function of z_0, the
characteristic surface roughness length; and L, the Monin-Obukhov
length, defined as follows:

$$L = \frac{u_*^3 c_p \rho T}{kgH} \tag{26}$$

where u_* is the friction velocity,

c_p is the specific heat of air at constant pressure,

ρ is the air density,

T is the absolute air temperature,

k is the von Karman's constant,

g is the acceleration of gravity,

H is the vertica heat flux.

In a now-classic paper by Golder (1972), these quantities
have been related to the Pasquill-Gifford stability classes.
During the BLM experiments, Schacher et al. (1982b) measured the
variables necessary to compute z_0 and L. Schacher et al.(1982a)
developed a modified Pasquill-Gifford classification (referred to
as NPS scheme) by relating z_0 and L to routine meteorological
measurements, and examined the behavior of σ_θ, the standard
deviation of the wind direction, as a function of the NPS scheme.
The analysis reported here extends this concept one step further,

59

using the NPS scheme of determining stability class together with actual trace gas measurements to build a family of curves.

The Schacher scheme requires four routine meteorological measurements to define stability class: mean windspeed, relative humidity, air temperature, and sea surface temperature. Three sets of curves, for 50%, 80%, and 95% relative humidity, are used to determine the class. Figure 14 shows the result for 50% humidity. From the air-sea temperature difference and the mean windspeed, an appropriate Pasquill-Gifford stability class is chosen by interpolation between curves. The complete set of algorithms is presented in Table 8. Two important points are, first, under this scheme, stability classes A, F, and G are not represented and second, the scheme breaks down at windspeeds under 2 m/s.

At windspeeds under 2 m/s, unless conditions are highly stable, turbulence, and therefore turbulent diffusion, becomes highly inhomogeneous on a horizontal plane. Defining a stability class in order to define plume spread for a Gaussian dispersion model implies homogeneous, steady-state conditions. Defining stability class A over the ocean is probably unnecessary, and may be inappropriate because it is unlikely the sea surface can supply upward heat flux capable of supporting extreme super-adiabatic conditions. Defining classes F and G, on the other hand, is important for coastal regions. Kristensen et al. (1981) gives many over-water examples where these conditions prevail for extended periods of time. Discussion of this problem is given in Appendix B.

60

FIGURE 14.

EXAMPLE OF NPS OVER-WATER STABILITY CLASSIFICATION SCHEME

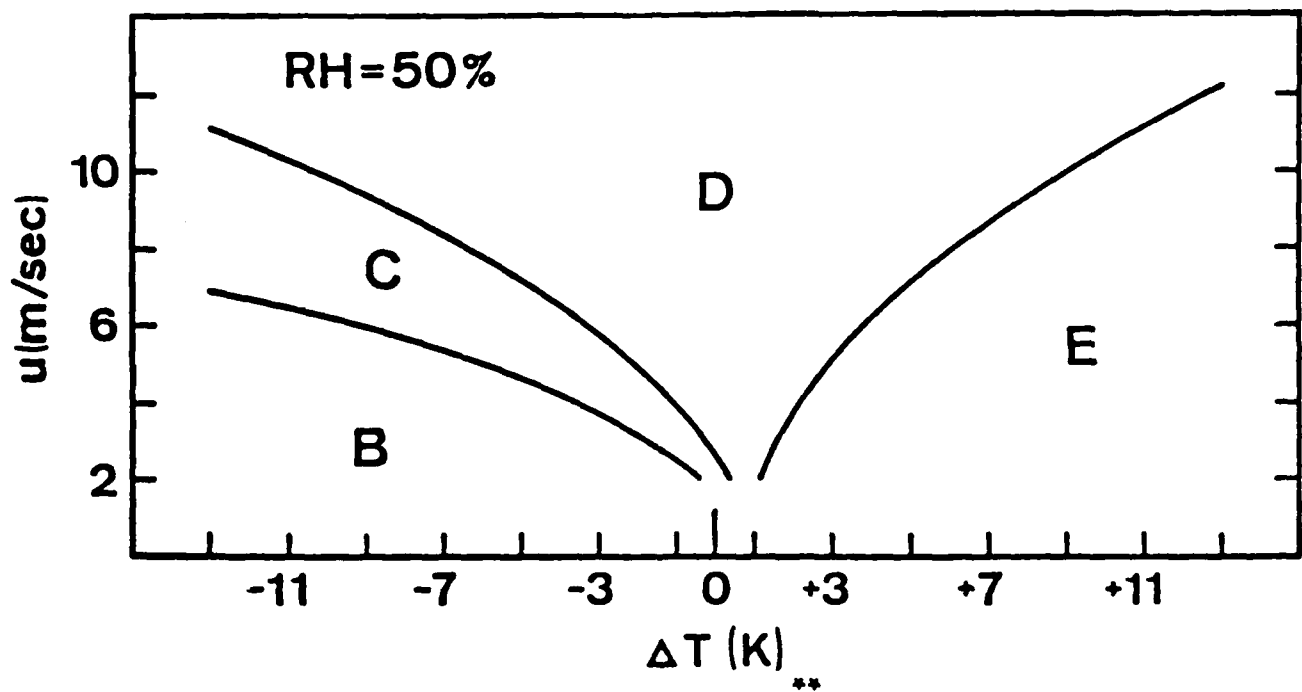** ΔT = air temperature - sea surface temperature

61

Table 8

P-G Stability Class Scheme
Adapted to a Marine Boundary Layer

$$U = a_0 + a_1 \Delta T + a_2 \Delta T^2 + a_3 \Delta T^3 + a_4 \Delta T^4$$

where a_0, a_1, a_2, a_4 are constants;
     U is windspeed;
     ΔT is (air temperature* - sea surface temperature) in °C

Relative Humidity	Boundary Line	a_0	a_1	a_2	a_3	a_4
50%	BC	1.59318	-0.95150	-0.09711	-0.00610	-0.00014
	CD	2.36805	-1.61613	-0.18965	-0.01315	-0.00031
	DE	-0.55452	2.65966	-0.34382	0.02783	-0.00087
80%	BC	1.12799	-1.08521	-0.11388	-0.00707	-0.00016
	CD	1.21695	-2.06787	-0.25450	-0.01708	-0.00040
	DE	0.56149	2.53558	-0.35185	0.03053	-0.00100
95%	BC	1.18368	-0.85413	-0.05274	-0.00248	-0.00005
	CD	1.12545	-1.79684	-0.16237	-0.00869	-0.00017
	DE	0.90463	2.74354	-0.47268	-0.04718	-0.00165

* Optimum: 10 meter measurement, but any surface layer value is
          acceptable.

The basic model used to parameterize plume growth for each stability category was

$$\sigma_{y,z}(x) = \sigma_{y,z} \text{ ref} \left(\frac{x}{x_{y,z \text{ ref}}} \right)^{\alpha,\beta} \tag{27a}$$

where $\sigma_{y,z}(x)$ is the horizontal or vertical standard deviation of the normally distributed mass at range X ;

$\sigma_{y,z}$ ref is a constant for a given stability category representing an appropriate $\sigma_{y,z}$ at a range $x_{y,z}$ ref;

α,β are constants for a given stability category representing horizontal or vertical plume growth.

For comparison with accepted overland models of similar form, $x_{y,z \text{ ref}}$ was chosen to be 100 m. To simplify notation, Equation 27a can be expressed as follows:

$$\sigma(x) = bx^c \tag{27b}$$

where $\sigma(x)$ is either σ_y or σ_z ,

b   is either σ_y ref$/(100)^\alpha$ or σ_z ref$/(100)^\beta$;

c   is either α or β.

The regression analysis was performed in several different fashions (to be discussed) for intercomparison, but all were designed to minimize the mean fractional error, defined as follows:

$$MFE = \frac{2(P-O)}{P+O} \tag{28}$$

63

where P is predicted plume parameter,

O is observed (measured) plume parameter.

Using this error analysis, instead of the usual mean square error, gives logarithmically unbiased results; an over-estimate of n x measured value is the same as an underestimate of $1/n$ x measured value. This implies that overpredictions are more heavily weighted than underpredictions. This is a desirable trait, since the data set has a lower, but no upper boundary. Also, the standard deviation of the MFE is a measure of the precision (scatter) of the estimate; another useful characteristic. Irwin (1982) gives a similar example of the use of MFE in a sensitivity analysis of overland dispersion models.

Equation 27b contains two unknowns. The coefficient b essentially represents the initial conditions, or short-range diffusion, which has not been measured directly over the ocean. The exponent, c, represents the curvature of the scatter plot, or the deviation from linearity of plume growth as a function of range. Regressing $\ln(\sigma(x))$ versus $\ln(X)$ and allowing both b and c to vary will not yield a unique solution. However, selecting a discrete set of values for either b or c will produce a single MFE minimum.

The first regression scheme attempted was to select a discrete set of values for c and examine the standard deviation of the MFE. In all cases σ_{MFE} varied only slightly, suggesting that there was no preferred combination of b and c.

Next, c was held constant and b allowed to vary. The value of c was chosen to be 0.85 for horizontal diffusion. This was based on a sensitivity study of various models as they apply to the Brookhaven over-water oil smoke experiment conducted off Long Island (Michael et al. [1973]). The study suggested the 0.85 value to be appropriate for all stability classes. Over land, c varies from about 0.80 for Pasquill-Gifford (P-G) class E to 1.00 for classes G-A. In most cases, holding c constant produced unreasonable values of b. In other words, the model misrepresented short-range diffusion.

To remedy the problem, the approach was reversed; estimates of short-range diffusion were assumed and the curvature term forced. As previously mentioned, no short-range diffusion data are available. However, statistical theory introduced by Taylor (1921) and applied by Pasquill (1971) and Draxler (1976) allow estimates of short-range diffusion. Specifically, in the horizontal case,

$$\sigma_y(T) = \sigma_v \, T \, f_y\left(\frac{T}{t_L}\right) \tag{29}$$

where σ_v is the standard deviation of the cross-wind velocity component;

T is the diffusion time;

$f_y\left(\frac{T}{t_L}\right)$ is a universal function;

t_L is the Lagrangian time scale.

Approximating $\sigma_v T \approx \sigma_\theta x$

$$\sigma_y(x) = \sigma_\theta x f_y \left(\frac{T}{t_L}\right) \tag{30}$$

where σ_θ is the standard deviation of the wind direction,

x is the downwind distance.

Sheih (1981) has experimentally determined the "universal" function over Lake Michigan for various P-G categories from trajectories of neutrally-buoyant balloons in the surface layer. Sheih (1981) used the model:

$$f_y \left(\frac{T}{t_L}\right) = \left[1 + \left(\frac{T}{2t_L'}\right)^{1/2}\right]^{-1} \tag{31}$$

where t_L' is an "apparent" integral time scale.

Table 9 lists Sheih's experimentally-determined "apparent" integral time scales and Draxler's overland equivalent. Draxler only separated data into stable or unstable; therefore, no "D" value is presented. Notice the large time scale in neutral conditions, representing a large "memory" of an air parcel's trajectory. This is probably a response to synoptic scale disturbances. In non-neutral conditions, the time scale is significantly less than the over-land counterpart.

Equations 30 and 31 can be used with measured values of σ_θ to obtain horizontal short-range parameters. The σ_θ values

66

Table 9.

Sheih's Apparent Integral Time Scales

P-G CLASS

	C	D	E
	(all values in seconds)		
horizontal	372 ± 29(617)	4056 ± 223	70.3 ± 3.2(617)
vertical	10.6 ± 1.1(309)	31.5 ± 2.1	21.7 ± 1.3(617)

(   ) Draxler's over-land results

•••

Table 10.

Horizontal and Vertical Wind Variance Values[*] from

Central California Air Quality Studies III and IV

P-G Class	# Hrs	1 Hr $\overline{\sigma_\theta}$	1 Hr $\overline{\sigma_\phi}$	1 min $\overline{\sigma_\theta}$	σ_θ Gifford (76)
B	10	31.0	11.8	7.2	20
C	10	17.3	9.8	7.3	15
D	129	9.1	3.3	2.6	10
E	36	12.6	1.5	2.1	5

* all values in degrees, and measured at 10 m.

67

obtained during the 3rd and 4th Central California experiments used for this procedure are summarized in Table 10. The sample time was one second, and the averaging period was one hour. Also included are the one-minute averaging period values and Gifford's (1976) values for comparison. Note that the over-water values agree with over-land values in all classes except class E. Inspection of the time series and statistical comparison with the well-known "t-distribution" indicates that the large σ_θ values of class E are statistically significant. These data are probably a large-scale phenomenon, since the one-minute values do not reveal relatively large class E values.

For the vertical case, values of σ_ϕ, the standard deviation of the vertical wind direction component, were not measured. They were, however, calculated using surface layer similarity from Binkowski (1978).

$$\sigma_\phi = \frac{u_*}{u} \left[\frac{\phi_m - z/L}{1.2\ f_M} \right]^{1/3} \qquad \text{for } z/L > 0 \qquad (32)$$

$$\phi_m = 1 + 5\ z/L \qquad (33)$$

$$f_M = 0.4 \left[1 + 3.39\ z/L - 0.25(z/L)^2 \right] \text{ for } 0 < z/L < 2.0 \qquad (34)$$

68

$$f_M = 0.4\left[6.78 + 2.39(z/L - 2.0)\right] \quad \text{for } z/L \geqslant 2.0 \tag{35}$$

$$\sigma_\phi = \frac{2.89}{u} h^{-.333} \quad \text{for } z/L < 0, \ h > 333 \text{ m} \tag{36}$$

$$\sigma_\phi = \frac{1.14}{u} h^{-.175} \quad \text{for } z/L < 0, \ 25 < h < 333 \text{ m} \tag{36}$$

where L   is the Monin-Obukhov length;

$u*$ is the friction velocity;

u   is 10 m windspeed;

h   is the inversion height.

As mentioned above, the reference distance used for the short range diffusion parameter, $\sigma_{y,z \text{ ref}}$, was 100 m. At this range, Equations 30-31 produce the results presented in Table 11. The minimum and maximum values result from deviations in the "universal function" due to uncertainties in the diffusion time (windspeed) and the apparent integral time scale (error margins in Table 9). Sheih (1981) did not present a value of t'_L for class B; therefore, values of Table 11 are based on "reasonable" t'_L values.

69

Table 11

Calculated $\sigma_{y,z \text{ ref}}$ values at 100 m.

	σ_y ref		(m.)		σ_z ref	
Class	min	mean	max	min	mean	max
B*	21.65	27.01	32.48	6.17	8.23	10.29
C	24.39	25.90	27.10	6.99	8.70	10.23
D	14.77	15.09	15.41	3.20	3.73	4.19
E	14.35	16.11	17.44	1.34	1.61	1.83

* only approximate

An interesting aspect of these results is that, for the horizontal case, the class D and E cases are very similar. This is the result of compensating influences of σ_θ and t_L; the smaller σ_θ values in class D are offset by the larger integral time scale (memory).

With the coefficient term of Equation 28 defined, the exponent can be forced in the regression analysis scheme. The results, the applications, and limitations are presented in the next chapter.

CHAPTER II - PRELIMINARY RESULTS

Additional Data Sets

Three additional data sets have been convolved with the data set described in this report (see Table 12). All experiments were conducted with continuous surface releases of the inert gas SF6. This implies that the parameterizations derived will be most applicable to a similar release. In addition, Dabberdt et al.(1983) produced some shoreline σ_y and σ_z values from the fourth Central California experiment (BLM IV) which are also incorporated into our data set. The first Gulf of Mexico experiment (GULF I) was conducted during the summer. The warm Gulf water produced the only P-G class B and C conditions that coincided with tracer releases. The third Central California experiment (BLM III) and GULF II were conducted in winter. Cool evening temperatures produced some unstable conditions during BLM III, but these events rarely coincided with tracer releases. GULF II was conducted during a stable, foggy period.

Table 12

ADDITIONAL DATA BASES FOR OVERWATER, MEDIUM-RANGE, SURFACE-RELEASE PLUME DISPERSION PARAMETERIZATION

EXPERIMENT	DATE	LOCATION	REFERENCE
Gulf of Mexico Air Quality Study I	Jul 81	Cameron, LA (area)	Dabberdt et al. (1982)
Central California Air Quality Study III	Dec 81	Pismo Beach, CA (area)	Dabberdt, et al. (1983)
Gulf of Mexico II	Feb 82	Cameron, LA (area)	Dabberdt, et al (1982)

71

The complete set of additional data and method of measurement is supplied in Table 13. Meteorological data is not tabulated, but stability categories were obtained in the manner described in this report.

Table 13

ADDITIONAL 1 HR AVERAGE PLUME PARAMETERS

-all values in meters

-all σ_z values from aircraft transects

-"s" indicates shoreline collectors for σ_y

-"a" indicates aircraft transects for σ_y

-"b" indicate grab bag samplers from boat

Experiment	Method	Date	HR	$\overline{\sigma_y}$	$\overline{\sigma_z}$	Range
BLM III	s	12-8-81	13	1225	21.5	6750
	s		14	455	18.5	6880
	s		15	644	15	6700
	s		16	1565	20	7320
	s	12-11-81	13	183	34	6560
	s		14	316	31.5	6630
	s		15	370	24	6660
	s		16	141	27	6660
	s		17	199	−	6820
	s		18	412	−	7190

Exp.	Method	Date	HR	$\bar{\sigma}_y$	$\bar{\sigma}_z$	Range
BLM III	s	12-17-81	12	--	216.5	6380
	s		13	231	17.5	6510
	s		14	332	-	6380
	s		15	677	116	6630
	s		16	299	39	6860
	s		17	154	22.5	6960
	s		18	387	-	7390
	s	12-14-81	12	194	18	6510
	s		13	200	22.5	6590
	s		14	187	23.5	6530
	s		15	176	12	6600
	s		16	224	-	6740
	s		17	784	-	7310
	s	12-15-81	12	601	79.5	7030
	s		13	346	42	6930
	s		15	723	14.5	6560
	s		16	268	16.5	7010
	s		17	458	35.5	7430
	s		18	812	___	8290

Exp	Method	Date	HR	$\bar{\sigma}_y$	$\bar{\sigma}_z$	Range
BLM IV	s	6-21-82	13	559	96	6590
	s		14	148	94.5	6590
	s		15	388	75.5	6640
	s		16	397	76	6670
	s		17	725	—	6590
	s	6-22-82	14	97	11	6280
	s		15	338	41	6380
	s		16	442	42.5	6300
	s		17	241	51.5	6160
	s		18	672	—	6160
	s		19	542	—	6180
	s	6-24-82	12	768	32	6430
	s		13	495	-	6330
	s		14	422	50.5	6280
	s		15	243	48	6250
	s		16	345	-	6290
	s		17	326	-	6590

EXP	Method	Date	HR	$\bar{\sigma}_y$	$\bar{\sigma}_z$	Range
BLM IV	s	6-25-82	11	117	___	6220
	s		12	219	30	6220
	s		13	260	55	6220
	s		14	239	36.5	6220
	s		15	149	46.5	6240
	s		16	156	___	6260
	s		17	525	___	6430
	s	6-27-82	11	139	___	6820
	s		12	83	___	6610
	s		13	131	___	6670
	s		14	202	34	6630
	s		15	156	39	6650
	s		16	172	32	6720
	s		17	263	32	6640
GULF I	s	7-20-81	13	55	58.5	7019
	b		13	483	___	8661
	s		14	671	___	9275
	b		14	85	___	7480
	s		15	2088	___	8330
	b		15	305	___	6209

EXP	Method	Date	HR	$\bar{\sigma}_y$	$\bar{\sigma}_z$	Range
GULF I	s	7-20-81	16	450	53	8037
	b		16	161	___	5721
	s		17	169	39	9368
	b		17	1492	___	6934
	s	7-23-81	15	870	___	9646
	b		15	354	___	6258
	s		16	49ε	37	8820
	b		16	203	___	6374
	s		17	233	38.5	8639
	b		17	750	___	5829
	b	7-27-81	19	687	___	6880
	b		19	710	___	5741
	b		20	451		7385
	b		20	108		6159
	s		21	142		7822
	s		21	124		5107
	s	7-27-81	13	381	___	8179
	s		13	104	___	5949
	s		14	608	107.5	8055
	s		15	496	115	7872
	b		15	69	___	8501
	s		16	565	___	8058
GULF II	s	2-15-82	13	333	17	4529
	a		13	92	___	2054
	a		13	39	___	1696
	s		14	147	11.5	3992

EXP	Method	Date	HR	$\bar{\sigma}_y$	$\bar{\sigma}_z$	Range
GULF II	a	2-15-82	14	68	____	1704
	s		15	679	____	5170
	s		16	543	____	5788
	s		17	268	____	4687
	s		18	125	____	4507

EXP	Method	Date	HR	$\bar{\sigma}_y$	$\bar{\sigma}_z$	Range
GULF II	s	2-15-82	19	108	—	4456
	s	2-17-82	13	121	—	6999
	s		14	624	—	6962
	s		15	783	—	7413
	s		16	329	—	7268
	s		17	692	—	6897
	s		18	675	—	7046
	s	2-22-82	12	289	9	7607
	a		12	419	—	4205
	a		12	531	—	4272
	a		12	51	—	4398
	s		13	368	7	7080
	a		13	394	—	3907
	a		13	219	—	3921
	a		13	389	—	4009
	s		14	455	21	6994
	a		14	197	—	3848
	a		14	184	—	3854
	a		14	63	—	3847
	s		15	161	—	7062
	s		16	88	13.5	6957
	a		16	238	—	3846
	a		16	179	—	6401
	a		16	236	—	3847

EXP	Method	Date	HR	$\bar{\sigma}_y$	$\bar{\sigma}_z$	Range
GULF II	s	2-22-82	17	592	31	6911
	a		17	70	—	3883
	a		17	573	—	4298
	a		17	389	—	3863
	s		18	211	—	7076

EXP	Method	Date	HR	$\bar{\sigma}_y$	$\bar{\sigma}_z$	Range
GULF II	s	2-23-82	10	498	——	7847
	s		11	238	76.7	7724
	a		11	146	——	4265
	a		11	349	——	4360
	a		11	139	——	4662
	s		12	471	33	8035
	a		12	109	——	4631
	s		12	145	——	4553
	a		12	115	——	4633
	s		13	179	53	7741
	a		13	89	——	4343
	a		13	198	——	4370
	a		13	163	——	4411
	s		14	117	——	7912
	s		15	315	57.7	7984
	a		15	295	——	4545
	a		15	268	——	4546
	a		15	490	——	4044
	s		16	489	46.7	7309
	a		16	395	——	4106
	a		16	313	——	4105
	a		16	490	——	4044
	s		17	107	33.5	7494
	a		17	116	——	7188
	a		17	99	——	7123
	s		18	101	——	7505

EXP	Method	Date	HR	$\bar{\sigma}_y$	$\bar{\sigma}_z$	Range
GULF II	s	2-24-82	14	186	12	5740
	a		14	163	——	2153
	a		14	139	——	2134
	s		15	186	13	5709
	a		15	123	——	2174
	a		15	105	——	2045
	s		16	83	11.5	6059
	a		16	82	——	2251
	a		16	47	——	2239
	s		17	279	10.5	5822
	a		17	148	——	2160
	a		17	137	——	1975
	s		18	102	——	4722
	s		19	172	——	5155

Vertical Dispersion Parameters

The encouraging results of the vertical dispersion parameterization are the well-behaved form of σ_z and the distinct difference between classes D and E. The discouraging aspect is that this data contains no class B or C values for σ_z. Figure 15 shows the BLM IV scatter plots and regression curves for classes D and E. Numerical results are presented in Table 14. Also shown is the Turner (1970) overland curves for comparison. The figure shows obvious differences between classes and a general slower overwater growth compared to its overland counterpart. The slower vertical growth is physically realistic when we consider surface roughness. Lower values of z_0 overwater produce smaller vertical velocity fluctuations during stable and neutral conditions, and therefore smaller plume parameters. The additional data sets were not included in the regression analysis. The Gulf data, by the author's admission, showed serious mass balance problems. Both data sets were based on airplane transects over the shoreline, where the internal boundary layer could have altered results. Nonetheless, this data is included in Figure 16 for review, and supports our results. As stated above, tracer data did not coincide with periods of class B or C stability. Meteorological data, however, was logged for 20 complete hours during these conditions (10 hours apiece). Based on the calculated vertical wind variance for these classes, and the well-behaved vertical dispersion in the neutral and stable
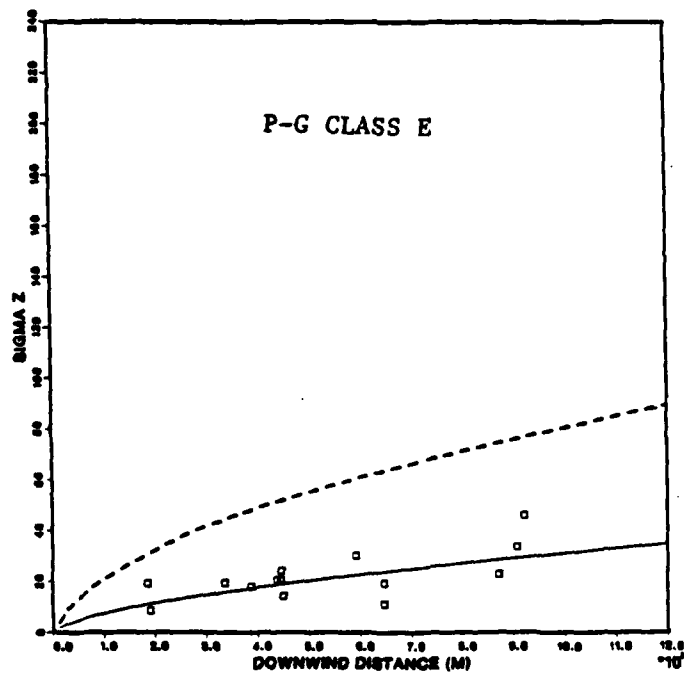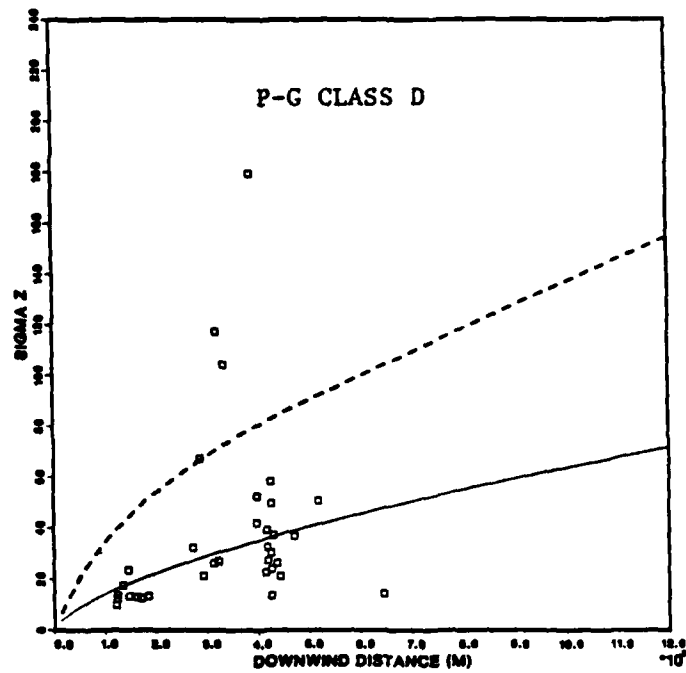
82

FIGURE 15. ONE HOUR AVERAGE VERTICAL PLUME PARAMETER FROM CCAQ IV

dashed line is Pasquill-Gifford
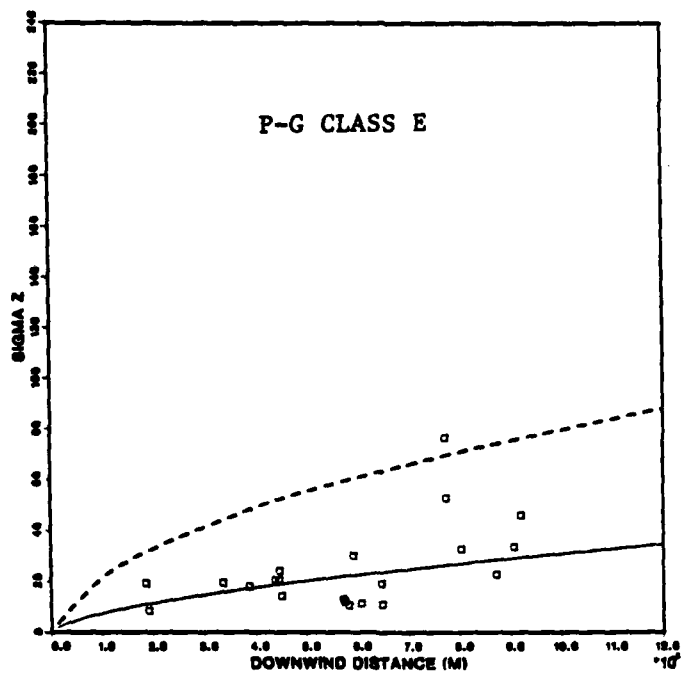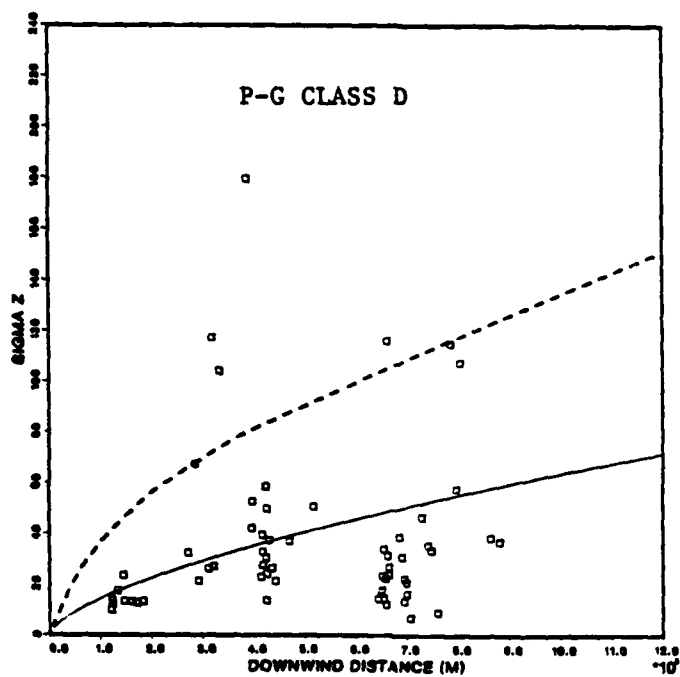
solid line is table (13)

FIGURE 16. ONE HOUR AVERAGE VERTICAL PLUME PARAMETER FROM
CCAQ IV AND TABLE (11) DATA SETS

dashed line is Pasquill-Gifford

solid line is table (13)

84

Table 14

ONE-HOUR AVERAGE PARAMETERIZATION FOR OVERWATER, SURFACE-RELEASE, MODERATE-RANGE* DISPERSION WITH OVERLAND** COMPARISON

$$\sigma_{y,z}(x) = \sigma_{y,z \ ref} \left(\frac{x}{x_{ref}}\right)^{\alpha, \beta}$$

$x_{ref} = 100$ m.

P-G Category	Over-water σ_y ref	Over-land σ_y ref	Over-water σ_z ref	Over-land σ_z ref	Over-water α	Over-land α	Over-water β	Over-land β
B	25.0	19.0	10.0	11.0	0.75a	1.00	0.75a	1.0
C	20.0	12.5	8.0	7.5	0.70a	1.00	0.70a	0.90
D	15.1	8.0	3.2	4.5	0.69	0.90	0.65	0.85
E	16.1	6.0	1.8	3.5	0.65	0.80	0.62	0.80

a insufficient data for verification
* moderate-range is 0.1-12 km
** Overland values from DTIC (1980)

categories, the shape of the σ_z curve is postulated in Table 14. Verification will proceed as unstable, overwater data become available to the NPS Environmental Physics Group.

Horizontal Dispersion Parameters

The hourly averaged horizontal tracer data for P-G classes D and E with regression lines are shown in Figure 17. These results are aesthetically less pleasing than the vertical case because of the increased scatter, but some differences between cases are noteworthy. First, the increased short-range diffusion due to meander for class E, predicted by the theory of the previous section, appears to be realistic when examining the clusters in the 1-2 km range. Second, clusters at greater ranges suggest the overall larger diffusion under class D conditions. The difference is small, however, and the parameterizations of Table 13 reflect this fact. As with the vertical data, P-G classes B and C were insufficiently dense. Ten data points were available in class C, seven in class B, and all data were from GULF I. No regression was attempted on these data, and the values in Table 13 were hypothesized, based on the meteorological (σ_θ) data. Verification is needed.
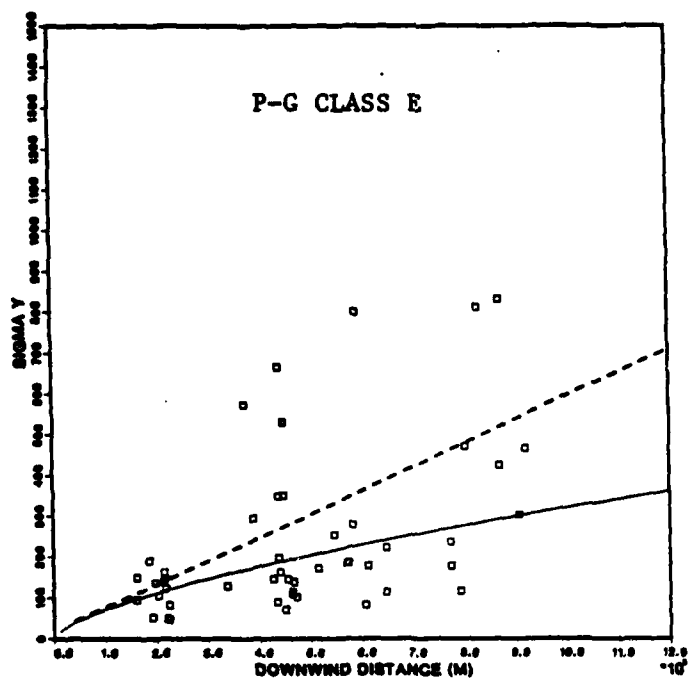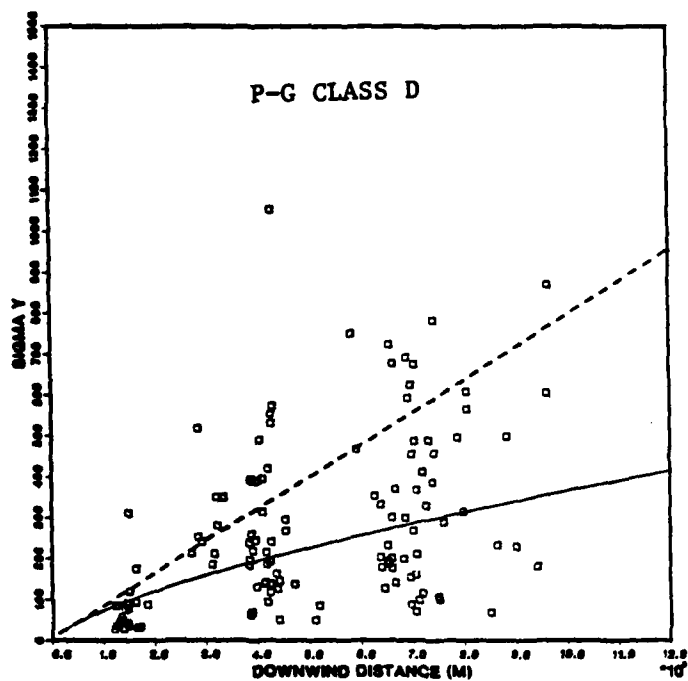
FIGURE 17. ONE HOUR AVERAGE HORIZONTAL PLUME PARAMETERS
FROM CCAQ IV AND TABLE (11) DATA SETS

dashed line is Pasquill-Gifford

solid line is table (13)

As with most tracer data, the points were widely scattered about chosen regression lines. This characteristic feature can be partially attributed to the highly variable nature of turbulence in the atmosphere. Another factor that significantly increases scatter for horizontal data is the large energy in the low frequency part of the horizontal velocity spectra. While a formal spectral analysis of the wind time series was not performed, variance did significantly increase with longer sampling windows, up to one hour. The time series also suggests that this trend would have continued with a larger window. A variety of overland experiments have observe: larje horizontal wind variance during stable conditions [Hanna (1981), Olesen et al. (1983), Sagendorf and Dickson (1974)]. Spectral analysis by Hanna (1981) indicated a low frequency peak at approximately 0.5 hour^{-1}. Olesen et al. (1983) describe large contributions to the energy spectrum at frequencies as low as 0.35 hour^{-1}. Kristensen et al. (1981) described increased plume meander in very stable conditions resulting from these low frequency oscillations, and finds an inverse relationship with the mean windspeed (see Appendix B).

Based on the above references, it is not surprising to find a large meander component in the class E σ_y values. It is somewhat unexpected to find a large meander component in near-neutral (class D) stability. These findings are supported in part by Sheih's (1981) large Langrangian time scales in these conditions, which he has suggested is the result of "large scale motions."

88

Regardless of the mechanisms involved in the low frequency wind fluctuations, their existence implies that one hour averages are inappropriate for defining horizontal "steady-state" diffusion.
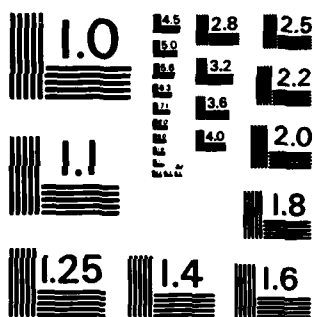
MICROCOPY RESOLUTION TEST CHART

NATIONAL BUREAU OF STANDARDS-1963-A

APPENDIX A

CENTRAL CALIFORNIA AIR QUALITY EXP. IV DATA

The methodology of this analysis was designd in a step-wise fashion to facilitate easy re-analysis. All data sets listed in Table 1A are semi-permanently logged at the NPS Computer Center. Nine-track digital tapes are also available. For the exact data set formats, contact this report's author.

TABLE 1A - TRACER EXPERIMENT DATA SETS AVAILABLE AT NPS

Analysis Step	Program Name	Output Data Set Name	Brief Description	Line#	Ordered content
1	FORMAT	AIR2	raw data	1	code, date time, pass#, data quality index, average altitude
				2	code, elapsed time, #of points, # of transponder 1 pts, # of transponder 2 pts, # bad pts
				3-end	code, mini-ranger#, mini-ranger distance, analyzer output
1	REDUCE	AIR3	calibrated data, rectangular coordinates	1	date,time, pass# #points
				2	plane heading, airspeed
				3	wind direction,wind speed
				4	standard deviation of output data
				5	cross-wind integrated concentration
				6	transect altitude
				7	distance from release
				8-11	mini-ranger statistics
				12	Release coordinates
				13	
				14-end	elapsed time, running plume width, e-w coordinate, n-s coordinate, concentration
2	XFORM	AIR4	untransformed, arranged data	1	date,time, pass#
				2	altitude, windspeed, wind direction
				3	plane heading, airspeed, distance from release
				4	release coordinates
				5	
				6-24	elapsed time, running plume width, e-w coordinate, n-s coordinate, concentration
2	XFORM	AIR5	transformed, averaged data		Same as AIR4

Analysis Step	Program Name	Output Data Set Name	Brief Description	line#	Ordered Content
3	MINIFIX	AIR6	corrected coordinates- untransformed data		same as AIR4
		AIR7	corrected coordinates- transformed data		same as AIR4
4	FIT	AIR8	multi-modal Gaussian fit	1	null
				2	plane heading, time
				3	altitude, distance from release
				4	e-w coordinate, n-s coordinate
				5	width position of mean mass
				6	standard deviation about mean
				7	total plume width
				8	null
				9	null
				10	peak#1 value, peak#2 value, etc.
				11	peak#1 position, peak# 2 position, etc
				12	peak#1 standard dev., peak#2 st. dev., etc.
5	BOTH	AIR9	hourly averages		See Appendix C for complete AIR9 output
6	BOTH	AIR12	AIR9 condensed	1	date, hour, relative humidity, wind direction, sigma theta
				2	windspeed, air temperature (10m.), sea-surface temperature, 10/L, inversion height
				3	1st average downwind distance (DWD), 1st standard deviation of DWD, 1st # of passes, 1st mean total sigma y
				4	1st mean waveform sigma y

92

Analysis Step	Program Name	Output Data Set Name	Brief Description	line#	Ordered Content
6	BOTH	AIR7	AIR9 condensed	4 cont.	1st fixed mean total sigma y from fits, 1st off-axis position of mean mass, 2nd average DWD, 2nd st. dev. of DWD
				5	2nd # of passes, 2nd mean total sigma y, 2nd mean waveform sigma y, 2nd fixed mean total sigma y from fits, 2nd off-axis position of mean mass
				6	3rd av. DWD, 3rd standard deviation of DWD, 3rd # of passes, 3rd mean total sigma y, 3rd mean waveform sigma y.
				7	3rd fixed mean total sigma y from fits, 3rd offaxis position of mean mass, 4th average DWD, 4th st. dev.of DWD, 4th# pas.
				8	4th mean total sigma y, 4th mean waveform sigma y, 4th fixed mean total sigma y from fits, offaxis position of mean mass, 1st mean total sigma y from fits
				9	1st weighted mean total sigma y from fits, 1st sigma z, 1st crosswind integrated concentration (CWIC), 2nd mean total sigma y from fits 2nd weighted mean total sigma y from fits
				10	fits 2nd sigma z, 2nd CWIC 3rd mean total sigma y from fits, 3rd weighted mean total sigma y from fits,

93

Analysis Step	Program Name	Output Data Set Name	Brief Description	line#	Ordered Content
6	BOTH	AIR12	AIR 9 condensed	11	3rd CWIC, 4th mean total sigma y from fits, 4th weighted mean total sigma y from fits, 4th sigma z, 4th CWIC
				12,13	null

Note: Identically formatted over-water data sets for Central California Air Quality Exp III and the two Gulf of Mexico experiments are also on file.

APPENDIX B

OVER-WATER PLUME DISPERSION IN VERY STABLE CONDITIONS

As stated in the main text, very stable conditions are not uncommon over the ocean. These conditions typically occur when the marine boundary layer capping inversions lowers to the sea surface. Under such conditions, the only true measure of stability is the atmospheric temperature lapse rate through the inversion. Dispersion in these conditions departs radically from traditional turbulent diffusion ideas. Kristensen et al. (1981) gives an elaborate theoretical discussion of the physics of dispersion in very stable conditions, identifying the key parameters as averaging time and mean windspeed. Using over-water tracer data at a 20km range, Kristensen found

$$\sigma_y \approx 3700 \ T^{1/3} \ U^{-4/5} \tag{1A}$$

where T is average time;

U is mean windspeed.

This formula is only valid at 20 km, and therefore is of little value to us, but demonstrates the convincingly changed character of diffusion in very stable conditions.

APPENDIX C

COMPLETE HOURLY AVERAGED PLUME PARAMETER INFORMATION FROM THE FOURTH

CENTRAL CALIFORNIA AIR QUALITY EXPERIMENT

(see Measured Plume Dispersion Parameters Over Water: Volume 2)

— available on request only —

References

1. F. S. Binkowski: A Simple Semi-empirical Theory for Turbulence in the Atmospheric Surface Layer,. Atmos. Environ. (1978)

2. D. Crow and L. Tewscher: Private communication. Aeroenvironment Corporation (1983)

3. W. F. Dabberdt, R. Brodzinsky, B. C. Cantrell, R. E. Ruff, R. Dietz, and S. SethuRaman: Atmospheric Dispersion Over Water and in the Shoreline Transition Zone: Vol 1 - Analysis and Results SRI3450. Stanford Research Institute, Menlo Park, California (1982)

4. W. F. Dabberdt, W. B. Johnson, R. Brodzinsky, and R. E. Ruff: Central California Coastal Air Quality Model Validation Study: Data Analysis and Model Evaulation. SRI Project 3868 [Draft (1983)]

5. Defense Technical Information Center: Methodology for Chemical Hazard Prediction, Department of Defense Explosives Safety Board, DTIC report # DDESB TP 10, Change 3 (1980)

6. R. R. Draxler: Determination of Atmospheric Diffusion Parameters. Atmos. Environ. $\underline{10}$, 99-105 (1976)

7. S. R. Hanna: Diurnal Variation of Horizontal Wind Direction Fluctuations in Complex Terrain at Geysers, California, Bound-Layer Meteor. $\underline{58}$, 207-213 (1981)

8. J. S. Irwin: Estimating Plume Dispersion - A Comparison of Several Sigma Schemes, Journal of Climate and Applied Meteorology $\underline{22}$, 92-114 (1982)

9. L. Kristensen, N. O Jensen, and E. L. Petersen: Lateral Dispersion of Pollutants in a Very Stable Atmosphere - The Effect of Meandering, Atmos. Environ. $\underline{15}$, 837-844 (1981)

10. P. Michael, G. S. Raynor, and R. M. Brown: Atmospheric Diffusion from an Off-shore Site, presented at IAEA Symposium No. 181 on the Physical Behavior of Radioactive Contaminants in the Atmosphere, Vienna, Austria, 12-16 Nov. 1973

11. H. R. Olesen, S. E. Larsen, and J. Hojstrup: Modeling Velocity Spectra in the Lower Part of the Planetary Boundary Layer, submitted to Boundary Layer Meteor. (1983)

12. F. Pasquill: Atmospheric Dispersion of Pollution, A. J. R. Met. Soc., $\underline{97}$, 369-395 (1971)

13. J. F. Sagandorf and C. R. Dickson: Diffusion Under Low Windspeed, Inversion Conditions. NOAA Tech. Memo ERL ARL-52, U. S. Dept. Commerce, p. 89 (1974)

14. G. E. Schacher, C. H. Reheis, D. E. Speil, and D. Crow: Analysis of Fine Scale Aircraft Data to Define Plume Structure, NPS-61-83-009PR (1983)

15. G. E. Schacher and C. W. Fairall: Comparison of Stability Classification Methods for Parameterizing Coasts Overwater Dispersion. First Int. Conference on Meteor. and Air/Sea Interaction of the Coastal Zone, the Hague, Netherlands, American Meteorological Society, Boston, Massachusetts (1982)

16. G. E. Schacher, D. E. Spiel, C. W. Fairall, K. L. Davidson, C. A. Leonard, and C. H. Reheis: California Coastal Offshore Transport and Diffusion Experiments - Meteorological Conditions and Data, NPS-61-82-007 (1982)

17. C. Sheih: Pasquill-Taylor Dispersion Parameters Overwater Near Shore, Atmos. Environ. 15, 101-105 (1981)

18. G. I. Taylor: Diffusion by Continuous Movements, Proc. London Math. Soc., 20, 196 (1921)

19. P. Zannetti, D. M. Wilbur, and R. A. Baxter: Southern California Offshore Air Quality Model Validation Study - Final Report AV-FR-81/559 (1981)

DISTRIBUTION LIST

		No. of Copies
1.	Defense Technical Information Center Cameron Station Alexandria, Virginia 22314	2
2.	Library, Code 0142 Naval Postgraduate School Monterey, California 93943	2
3.	Prof. K. L. Davidson, Code 63Ds Department of Meteorology Naval Postgraduate School Monterey, California 93943	1
4.	Prof. G. E. Schacher, Code 61Sq Department of Physics Naval Postgraduate School Monterey, California 93943	10
5.	Dr. Warren Johnson SRI International 333 Ravenswood Avenue Menlo Park, California 93025	1
6.	LT Betty Hagan SD/CFAT Headquarters Space Division Post Office Box 92960 Worldway Postal Center Los Angeles, California 90009	1
7.	Dr. Ray Bernberg The Aerospace Corporation Space Launch Vehicle Division Post Office Box 92957 Los Angeles, California 90009	1
8.	Dr. Ron Bywater The Aerospace Corporation Space Launch Vehicle Division Post Office Box 92957 Los Angeles, California 90009	1
9.	Dr. Ron Cionco Atmospheric Sciences Lab WSMR, New Mexico 80002	1
10.	Dr. Abel Blanco Atmospheric Sciences Lab WSMR, New Mexico 80002	1

11. Dr. Paul Tag   2
    Naval Environmental Prediction Research Facility
    Monterey, California 93943

12. Mr. Sam Brand   1
    Naval Environmental Prediction Research Facility
    Monterey, California 93943

13. Dr. Steven Hannah   1
    Principal Meteorologist
    Environmental Research & Technology Corp.
    696 Virginia Road
    Concord, Massachusetts 01742

14. Mr. Don Spiel, Code 61   1
    Department of Physics
    Naval Postgraduate School
    Monterey, California 93943

15. Mr. Chuck Skupniewicz, Code 61   20
    Department of Physics
    Naval Postgraduate School
    Monterey, California 93943

16. CDR S. G. Colgan   2
    Code 420 B
    Office of Naval Research
    800 N. Quincy Street
    Arlington, Virginia 22217

17. MAJ Gary G. Worley   1
    Air Force Engineering and Services Center
    AFESC/RDVA
    Tyndall Air Force Base, Florida 32403

18. Dr. Dirk Herkoff   2
    Pacific Outer Continental Shelf Office
    Minterals Management Service
    1340 W. 6th Street, Room 200
    Los Angeles, California 90017

19. Dr. Donald L. Shearer   1
    TRC Environmental Consultants, Inc.
    8775 E. Orchard Road, Suite 816
    Englewood, Colorado 80111

20. Mrs. Patricia Boyle, Code 63Bp   1
    Department of Meteorology
    Naval Postgraduate School
    Monterey, California   93943

21. Mr. Peter Guest, Code 63Gp
    Department of Meteorology   1
    Naval Postgraduate School
    Monterey, California 93943

22. Mr. Thomas Rappolt   1
    Titen Systems Inc.
    8950 Villa La Jolla Drive
    Suite 2232
    La Jolla, California 92038

23. Mr. Dan Goddin   1
    ERT
    975 Business Center Circle
    Newbury Park, California 21320

24. LCDR James D. Branum   2
    2682 Olivestone Way
    San Jose, California 95132

25. Mr. Lyn Tewscher   1
    Titen Systems Inc.
    8959 Villa La Jolla Drive
    La Jolla, California 92038

26. Dr. Welf Aufm Kampe   1
    German Military Geophysical Office
    Mont Royal
    D-5580 Traben-Trarbach
    FEDERAL REPUBLIC OF GERMANY

27. Office of Naval Research   2
    (Attn: CDR S. Colgan, Code 420B)
    800 N. Quincy Street
    Arlington, Virginia 22217

28. Office of Naval Research   1
    (Attn: Dr. Robert Abbey, Code 425MM)
    800 N. Quincy Street
    Arlington, Virginia 22217

END

FILMED

1-85

DTIC